

Lipid signalling drives proteolytic rewiring of mitochondria by YME1L

<https://doi.org/10.1038/s41586-019-1738-6>

Received: 4 December 2018

Accepted: 19 September 2019

Published online: 6 November 2019

Thomas MacVicar^{1,9}, Yohsuke Ohba^{1,9}, Hendrik Nolte^{1,2}, Fiona Carola Mayer¹, Takashi Tatsuta¹, Hans-Georg Sprenger^{1,2}, Barbara Lindner², Yue Zhao³, Jiahui Li³, Christiane Bruns³, Marcus Krüger^{2,4}, Markus Habich⁵, Jan Riemer⁵, Robin Schwarzer², Manolis Pasparakis^{1,2,4}, Sinika Henschke⁶, Jens C. Brüning^{4,6,7}, Nicola Zamboni⁸ & Thomas Langer^{1,2,4*}

Reprogramming of mitochondria provides cells with the metabolic flexibility required to adapt to various developmental transitions such as stem cell activation or immune cell reprogramming, and to respond to environmental challenges such as those encountered under hypoxic conditions or during tumorigenesis^{1–3}. Here we show that the *i*-AAA protease YME1L rewires the proteome of pre-existing mitochondria in response to hypoxia or nutrient starvation. Inhibition of mTORC1 induces a lipid signalling cascade via the phosphatidic acid phosphatase LIPIN1, which decreases phosphatidylethanolamine levels in mitochondrial membranes and promotes proteolysis. YME1L degrades mitochondrial protein translocases, lipid transfer proteins and metabolic enzymes to acutely limit mitochondrial biogenesis and support cell growth. YME1L-mediated mitochondrial reshaping supports the growth of pancreatic ductal adenocarcinoma (PDAC) cells as spheroids or xenografts. Similar changes to the mitochondrial proteome occur in the tumour tissues of patients with PDAC, suggesting that YME1L is relevant to the pathophysiology of these tumours. Our results identify the mTORC1–LIPIN1–YME1L axis as a post-translational regulator of mitochondrial proteostasis at the interface between metabolism and mitochondrial dynamics.

The metabolic functions of mitochondria are coupled to changes in their morphology that are shaped by opposing fusion and fission events⁴. The *i*-AAA protease YME1L in the inner membrane balances fusion and fission by processing the dynamin-like GTPase OPA1^{5–9}. *YME1L*^{−/−} cells showed strongly impaired anchorage-independent growth, which mimics detachment from the extracellular matrix and exposes cells to nutrient and oxygen gradients that lead to metabolic rewiring. Cell growth was restored upon expression of YME1L but not in the presence of proteolytically inactive YME1L (YME1L(E543Q)) (Fig. 1a). Similarly, growth of spheroids in 3D was reduced in the absence of YME1L (Extended Data Fig. 1a–d). However, *YME1L*^{−/−} cells did not show deficiencies in basal oxygen consumption rate (Fig. 1b) or changes in the NAD⁺/NADH ratio, and spheroid growth was not restored when the NAD⁺/NADH ratio was increased (Extended Data Fig. 1e, f).

Because cells within spheroids consume both glucose and glutamine¹⁰, we tested whether *YME1L*^{−/−} cells could use glutamine for growth. Supplementation with glutamine stimulated the growth of cells containing YME1L, but not that of *YME1L*^{−/−} cells (Fig. 1c). Glutamine-dependent respiration was higher in wild-type than in *YME1L*^{−/−} cells (Fig. 1b, d), whereas both cell types showed a similar dependency on glucose and fatty acid oxidation (Extended Data Fig. 1g). Glutamine can serve as an alternative source of carbon to the TCA cycle to maintain

citrate levels, which is of particular importance to cells forced to grow in anchorage-independent conditions¹⁰. We observed substantially reduced levels of (iso)-citrate and aconitate in *YME1L*^{−/−} cells, whereas other TCA cycle intermediates remained largely unaltered (Extended Data Fig. 1h). Moreover, glutamine-derived metabolites such as glutamate and aspartate were diminished in *YME1L*^{−/−} cells, whereas glutamine itself and other amino acids were not affected (Extended Data Fig. 1i, j). These results are consistent with a requirement for YME1L in efficient glutamine utilization and point to insufficient replenishment of the TCA cycle in *YME1L*^{−/−} spheroids.

YME1L reshapes mitochondrial proteome in hypoxia

The requirement of YME1L for spheroid formation suggests that metabolic rewiring depends on the proteolysis of mitochondrial proteins. We observed substantially reduced levels of known substrates of YME1L (such as PRELID1, OPA1 and TIMM17A) in spheroids compared to monolayer cells (Fig. 1e). The steady-state concentrations of these proteins were increased and maintained at similar levels in cells lacking YME1L or expressing YME1L(E543Q), regardless of whether cells were cultivated in monolayers or grown in spheroids (Fig. 1e).

¹Max-Planck-Institute for Biology of Ageing, Cologne, Germany. ²Institute of Genetics and Cologne Excellence Cluster on Cellular Stress Responses in Aging-Associated Diseases (CECAD), University of Cologne, Cologne, Germany. ³Department of General, Visceral and Cancer Surgery, University Hospital of Cologne, Cologne, Germany. ⁴Center for Molecular Medicine, University of Cologne, Cologne, Germany. ⁵Institute for Biochemistry, University of Cologne, Cologne, Germany. ⁶Max-Planck-Institute for Metabolism Research, Cologne, Germany. ⁷Center for Endocrinology, Diabetes and Preventive Medicine (CEPD), University Hospital of Cologne, Cologne, Germany. ⁸Molecular Systems Biology, ETH Zürich, Zürich, Switzerland. ⁹These authors contributed equally: Thomas MacVicar, Yohsuke Ohba. *e-mail: langer@age.mpg.de

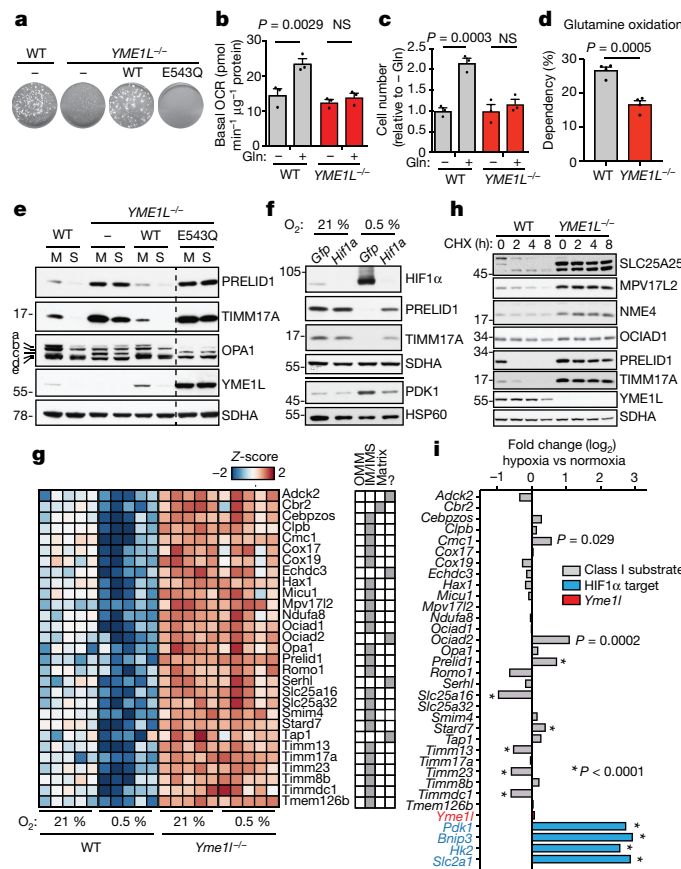


Fig. 1 | YME1L-mediated proteolysis is required for spheroid growth. **a**, Soft agar colony growth of wild-type (WT) and *YME1L*^{-/-} HEK293 cells, and *YME1L*^{-/-} HEK293 cells expressing WT YME1L or YME1L(E543Q). **b**, Basal oxygen consumption rates (OCR) of WT and *YME1L*^{-/-} HEK293 cells cultured in the absence or presence of 2 mM glutamine ($n=3$ independent experiments). **c**, Fold change in cell numbers of WT and *YME1L*^{-/-} HEK293 cells cultured in 2 mM glutamine ($n=3$ independent experiments). **d**, Dependency of WT and *YME1L*^{-/-} HEK293 cells on glutamine oxidation calculated as per cent of combined glucose, fatty acid and glutamine oxidation ($n=4$ independent experiments). **e**, Immunoblot of WT and *YME1L*^{-/-} HEK293 cells, and *YME1L*^{-/-} HEK293 cells expressing WT YME1L or YME1L(E543Q), cultured as monolayers (M) or spheroids (S) for 7 days (representative data from two independent experiments). Letters a–e represent different forms of OPA1. **f**, Representative immunoblot of HeLa cells transfected with esiRNA targeting *Gfp* or *Hif1α* cultured in normoxic or hypoxic conditions for 24 h. Quantification is shown in Extended Data Fig. 2e ($n=3$ independent experiments). **g**, Left, heatmap of Z -score of \log_2 -transformed label-free quantification (LFQ) intensities of class I YME1L substrate proteins in mitochondria of indicated MEF cells in normoxia and hypoxia ($n=5$ independent experiments). Right, mitochondrial compartmentalization. **h**, Immunoblot analysis of WT and *YME1L*^{-/-} HeLa cells treated with cycloheximide (CHX) for the indicated times (representative data from three independent experiments). **i**, Fold change (\log_2) of indicated mRNAs between hypoxia and normoxia in WT MEFs after 16 h ($n=3$ independent experiments; P values calculated using Benjamini–Hochberg method and indicated where $P < 0.05$). Means \pm s.e.m.; two-way analysis of variance (ANOVA) with Sidak multiple comparison test (**b**, **c**); two-tailed t -test (**d**); NS, not significant.

Cells within spheroids are exposed to hypoxic conditions, which suggests that YME1L may be regulated by a HIF1 α -dependent response (Extended Data Fig. 2a). YME1L substrates were diminished in wild-type cells undergoing hypoxia (0.5% O₂) or after treatment with HIF1 α -stabilizing agents, but remained elevated in *YME1L*^{-/-} cells and in cell lines treated with short interfering RNA (siRNA) targeting *Yme1l* (Extended Data Fig. 2b–d). Conversely, depletion of HIF1 α from hypoxic

wild-type cells stabilized YME1L substrates, demonstrating that HIF1 α is required to promote the loss of these proteins (Fig. 1f, Extended Data Fig. 2e). However, enhanced proteolysis by YME1L does not reflect transcriptional upregulation of *YME1L* (Fig. 1i). YME1L protein levels were decreased in cells grown in spheroids or under hypoxia (Fig. 1e, Extended Data Fig. 2a–c). This is likely to reflect autocatalytic degradation, as YME1L was stabilized in cells expressing YME1L(E543Q) (Fig. 1e, Extended Data Fig. 2b).

The selected set of mitochondrial proteins also decreased in hypoxic cells lacking ATG5¹¹, demonstrating that general autophagy does not explain their decreased levels (Extended Data Fig. 2f). Our results thus point to an enhanced and specific proteolytic response within mitochondria that occurs in a HIF1 α -dependent manner under hypoxia.

Quantitative proteomics revealed that there was a significant reduction in total mitochondrial protein content in wild-type mouse embryonic fibroblast (MEF) cells when they were shifted to hypoxia, but not in *Yme1l*^{-/-} cells (Extended Data Fig. 3a). Under normoxia, 64 mitochondrial proteins accumulated significantly in YME1L-deficient cells; these are likely to represent substrates of YME1L (Extended Data Fig. 3b, Extended Data Table 1). Using stringent selection criteria, we found that 29 of these putative YME1L substrates were downregulated under hypoxia in a YME1L-dependent manner (termed class I) (Fig. 1g, Extended Data Fig. 3c, d, Extended Data Table 1). Class I proteins included subunits of protein translocases, mitochondrial lipid transfer proteins, OPA1, and proteins that are functionally linked to mitochondrial metabolism. We confirmed that the protein stability of some substrates depended on YME1L in cycloheximide-treated cells (Fig. 1h), and transcriptomic analysis of normoxic and hypoxic cells revealed that the mRNA levels of the substrates were not collectively regulated by HIF1 α (Fig. 1i). We designated the remaining 35 putative YME1L substrates that accumulated in *Yme1l*^{-/-} cells during normoxia as class II (Extended Data Table 1). Thus, YME1L-mediated proteolysis broadly preserves mitochondrial proteostasis under normoxia and reshapes the mitochondrial proteome in response to hypoxia.

Hypoxia induced increased turnover of OPA1 by YME1L, indicating impaired mitochondrial fusion (Fig. 1g). Moreover, loss of YME1L resulted in activation of the second OPA1-processing peptidase, OMA1, in monolayer cells and spheroids, as indicated by the accumulation of OPA1 forms c and e⁸ (Fig. 1e). Deletion of *Oma1* suppresses mitochondrial fragmentation in *Yme1l*^{-/-} cells in vitro and in vivo^{6,8}, but did not affect the abundance of class I YME1L substrates in hypoxia (Extended Data Fig. 3e). We observed turnover of OMA1 by YME1L in hypoxic cells (Extended Data Fig. 3f), as observed in depolarized mitochondria¹². Depletion of OMA1 did not disturb spheroid growth or restore spheroid formation in the absence of YME1L (Extended Data Fig. 3g). Thus, impaired spheroid growth of YME1L-depleted cells is not a result of mitochondrial fragmentation inherent to these cells.

mTORC1 regulates YME1L-dependent proteolysis

Hypoxia and stabilization of HIF1 α inhibit mTORC1^{13–15}, which results in dephosphorylation of the downstream mTORC1 target ribosomal protein S6 in wild-type and *YME1L*^{-/-} cells (Extended Data Fig. 4a). Consistent with inhibition of mTORC1 regulating YME1L-mediated proteolysis, glutamine starvation—which is known to inhibit mTORC1^{13,14}—induced degradation of YME1L substrates (Extended Data Fig. 4b). YME1L substrates decreased in wild-type cells, but not in *YME1L*^{-/-} cells that were treated with the mTORC1 inhibitors rapamycin or Torin1 (Fig. 2a, Extended Data Fig. 4c, d).

mTOR forms two distinct signalling complexes—mTORC1 and mTORC2—that are characterized by the presence of RAPTOR (regulatory protein associated with mTOR) or RICTOR (rapamycin insensitive companion of mTOR), respectively^{13,14}. The levels of YME1L substrates were decreased in cells lacking RAPTOR (that is,

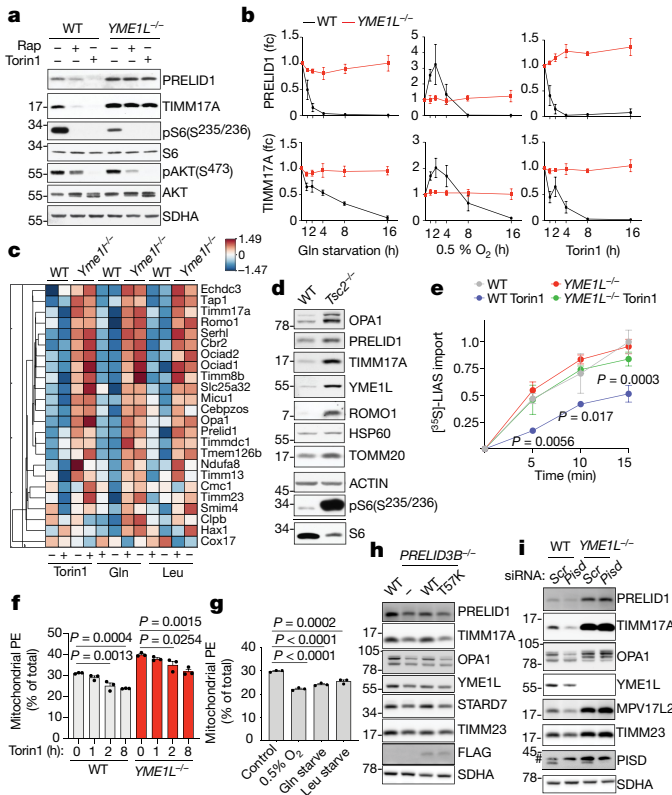


Fig. 2 | mTORC1 acutely regulates YME1L-dependent proteolysis and mitochondrial import. **a**, Immunoblot analysis of WT and *YME1L*^{−/−} HEK293 cells cultured in the presence of rapamycin (Rap) or Torin1 for 16 h (representative data from 3 independent experiments). **b**, PRELID1 and TIMM17A protein levels determined by immunoblotting of WT and *YME1L*^{−/−} HEK293 cells treated as indicated ($n=3$ independent experiments). **c**, Heat map of Z -scores of \log_2 -transformed LFQ intensities of class I YME1L substrate proteins detected in MEF cells treated as indicated. Z -scores calculated within each treatment ($n=4$ (Torin); $n=5$ (Gln and Leu) biological replicates). **d**, YME1L substrate expression in WT and *Tsc2*^{−/−} MEFs (representative data from three independent experiments). **e**, [35 S]-LIAS was imported into mitochondria isolated from WT and *YME1L*^{−/−} HEK293 cells after 18 h of treatment with or without Torin1. Import was initiated in the presence or absence of membrane potential ($\Delta\psi$) and analysed by SDS-PAGE and autoradiography. The level of [35 S]-LIAS imported into WT mitochondria after 15 min was set to 1 ($n=3$ independent experiments; mean \pm s.d.). **f**, **g**, Analysis of mitochondrial phospholipids in HeLa cells treated with Torin1 ($n=3$ independent experiments) (**f**) and HEK293 cells after hypoxia (0.5% O₂) or in glutamine- or leucine-depleted medium for 16 h (**g**; $n=3$ independent experiments). **h**, **i**, Representative immunoblots of indicated HeLa cell lines. Protein quantification is shown in Extended Data Fig. 6e. **j** ($n=4$ (**h**) or 5 (**i**) independent experiments) # denotes nonspecific cross-reaction. Mean \pm s.e.m.; one-way ANOVA with Dunnett's multiple comparisons test (**e–g**). fc, fold change.

containing inactive mTORC1), whereas inactivation of mTORC2 by the loss of RICTOR did not destabilize YME1L substrates (Extended Data Fig. 4e).

Thus, inhibition of mTORC1 upon amino acid starvation or in hypoxia promotes YME1L-dependent proteolysis. Degradation of YME1L substrates occurred acutely upon glutamine starvation, during hypoxia and after mTOR inhibition (Fig. 2b, Extended Data Fig. 4a–c). After treatment of cells with Torin1 or during leucine or glutamine starvation, the levels of most YME1L substrates (class I) decreased in a YME1L-dependent manner (Fig. 2c). Moreover, stimulation of mTORC1 in *Tsc2*^{−/−} cells or upon addition of amino acids or insulin caused the accumulation of YME1L substrates¹⁶ (Fig. 2d, Extended Data Fig. 4f, g). Thus, mitochondrial proteolysis is acutely regulated by mTORC1: activation of

mTORC1 inhibits protein degradation by YME1L, whereas inhibition of mTORC1 promotes YME1L-mediated proteolysis.

The increased turnover of protein translocases by YME1L suggests that the proteolytic response acutely limits the import of proteins into mitochondria. We therefore assessed the import of 35 S-labelled mitochondrial matrix proteins lipoic acid synthase (LIAS) and superoxide dismutase 2 (SOD2) into mitochondria isolated from wild-type and *YME1L*^{−/−} cells treated with Torin1. Import rates were reduced in wild-type but not *YME1L*^{−/−} mitochondria (Fig. 2e, Extended Data Fig. 4h, i). Similarly, both proteins were imported less efficiently into mitochondria isolated from hypoxic wild-type cells but not *YME1L*^{−/−} cells (Extended Data Fig. 4j).

Thus, YME1L-mediated proteolysis acutely limits mitochondrial biogenesis upon mTORC1 inhibition by degrading protein translocases and lipid transfer proteins and metabolically rewrites pre-existing mitochondria to preserve the TCA cycle for anaplerotic reactions.

Decreased PE promotes YME1L proteolysis

mTORC1 regulates mitochondrial function via transcriptional and translational circuits^{17,18}. However, stimulation of YME1L-mediated proteolysis upon inhibition of mTORC1 occurs post-translationally (Fig. 1i, Extended Data Fig. 5). As mTORC1 promotes lipid biosynthesis to support membrane biogenesis¹⁹, alterations in the lipid composition of mitochondrial membranes resulting from inhibition of mTORC1 could explain increased proteolysis by membrane-anchored YME1L. Mitochondrial membranes isolated from Torin1-treated wild-type and *YME1L*^{−/−} cells contained less phosphatidylethanolamine (PE) than did those from untreated cells (Fig. 2f). The levels of other phospholipids and the acyl chain composition of PE did not change under these conditions (Extended Data Fig. 6a–c). Similarly, mitochondrial PE levels were decreased in hypoxic cells and in cells starved for glutamine or leucine (Fig. 2g). We also monitored YME1L substrates in cells depleted of PRELID3B (also known as SLMO2), a lipid transfer protein in the intermembrane space that shuttles phosphatidylserine (PS) to the inner membrane for conversion to PE by PISD²⁰. Knockout or knockdown of PRELID3B reduced mitochondrial PE levels (Extended Data Fig. 6d, g) and decreased levels of YME1L substrate proteins (Fig. 2h, Extended Data Fig. 6e, f). Expression of PRELID3B, but not of the transfer-inactive mutant PRELID3B(T57K), restored the levels of both PE and YME1L substrates (Fig. 2h, Extended Data Fig. 6e, h, i). Furthermore, depletion of PISD reduced mitochondrial PE levels²¹ and destabilized YME1L substrates (Fig. 2i, Extended Data Fig. 6j, k). Conversely, there was a significant increase in mitochondrial PE levels in *Tsc2*^{−/−} cells, which contain hyperactive mTORC1 and accumulate YME1L substrates (Fig. 2d, Extended Data Fig. 6l). These experiments suggest that a decrease in mitochondrial PE levels may activate YME1L-mediated proteolysis. Supplementation of Torin1-treated cells with ethanolamine or lyso-phosphatidylethanolamine (LPE) preserved mitochondrial PE (Extended Data Fig. 7a, c) and stabilized YME1L substrates (Fig. 3a, b, Extended Data Fig. 7b, d). LPE supplementation also restored mitochondrial PE levels and stabilized YME1L substrates in PISD-depleted cells (Extended Data Fig. 7e, f).

To directly monitor how PE levels affect YME1L-mediated proteolysis, we reconstituted the process in liposomes. YME1L and a substrate (TIMM17A or a variant of OPA1) were synthesized in a cell-free system in the presence of liposomes, and membrane-associated proteolysis was initiated by adding ATP (Fig. 3c). YME1L, but not YME1L(E543Q), degraded both substrate proteins in an ATP-dependent manner (Fig. 3d, Extended Data Fig. 7g, h). Decreasing PE levels in liposomes from 34% to mimic the PE concentration in the inner membrane caused increased proteolysis of TIMM17A and OPA1, whereas increasing PE levels in liposomes stabilized both substrates (Fig. 3e, Extended Data Fig. 7i, j). We therefore conclude that mTORC1 signalling regulates PE levels in mitochondria, and that this determines protein

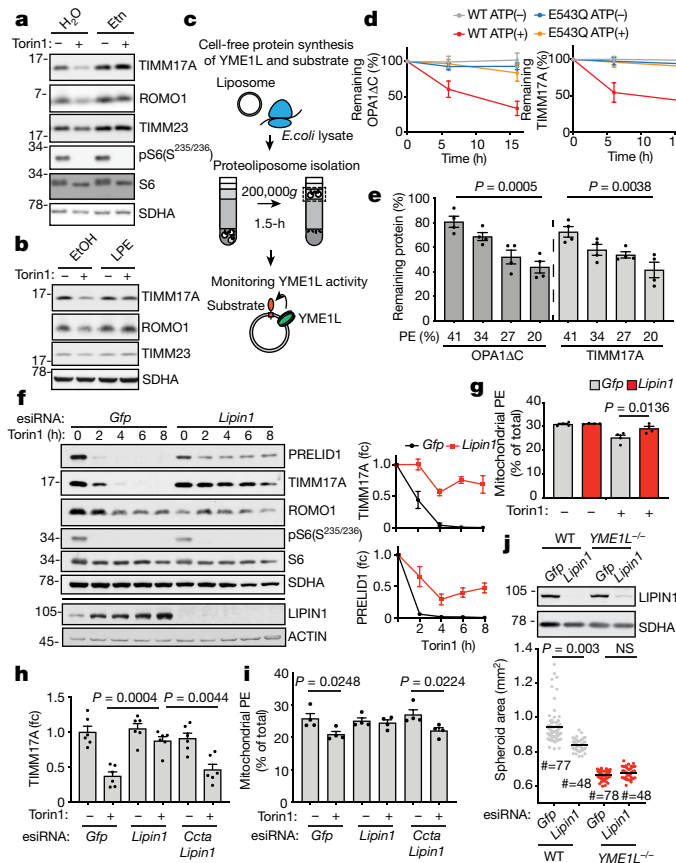


Fig. 3 | mTORC1 regulates mitochondrial PE in a LIPIN1-dependent manner. **a, b**, HeLa cells treated with Torin1 for 4 h followed by 24 h ethanolamine (Etn, 200 μ M) treatment (**a**) and HEK293 cells treated with Torin1 and/or LPE (100 μ M) for 4 h (**b**). Protein quantification is shown in Extended Data Fig. 7b, d ($n = 5$ independent experiments). **c**, Workflow for reconstitution of membrane-associated proteolysis by YME1L. **d**, YME1L (WT or E543Q) and its substrate, either OPA1 Δ C or TIMM17A, were reconstituted in liposomes and incubated in the presence or absence of ATP ($n = 3$ independent experiments). **e**, YME1L-mediated proteolysis in liposomes containing different amounts of PE. Proteoliposomes were incubated in the presence of ATP for 6 h (OPA1 Δ C) or 16 h (TIMM17A) ($n = 4$ independent experiments). **f, g**, Immunoblot and phospholipid analysis from HeLa cells transfected with esiRNA against *Gfp* or *Lipin1* and treated with Torin1 for the indicated time. Levels of PRELID1 and TIMM17A and mitochondrial PE after 4 h Torin1 treatment are shown ($n = 4$ independent experiments). **h, i**, Immunoblot quantification and phospholipid analysis from indicated esiRNA transfected HeLa cells treated with Torin1 for 4 h. TIMM17A protein levels ($n = 6$ independent experiments) and mitochondrial PE levels ($n = 4$ independent experiments) are shown. **j**, Spheroid surface area of WT and *YME1L* $^{-/-}$ HEK293 cells treated with *Gfp* or *Lipin1* esiRNA ($n = 3$ independent experiments; # denotes number of spheroids). Representative immunoblot of protein levels after 4 days is shown. Mean \pm s.e.m.; one-way ANOVA (**e**), two-way ANOVA with Tukey's (**g–i**) or Sidak's (**j**) multiple comparisons tests. fc, fold change.

degradation by YME1L. The exact mechanism by which PE affects proteolysis by YME1L remains unclear. YME1L assembles with the membrane scaffold SLP2 into the SPY complex²². Therefore, spatially restricted YME1L and local changes in PE may explain how modest alterations in mitochondrial PE upon inhibition of mTORC1 can lead to a robust and rapid proteolytic response.

LIPIN1-dependent phospholipid signalling

We used endoribonuclease-prepared siRNA (esiRNA) to suppress five mTORC1 target proteins that are known to regulate cellular lipid

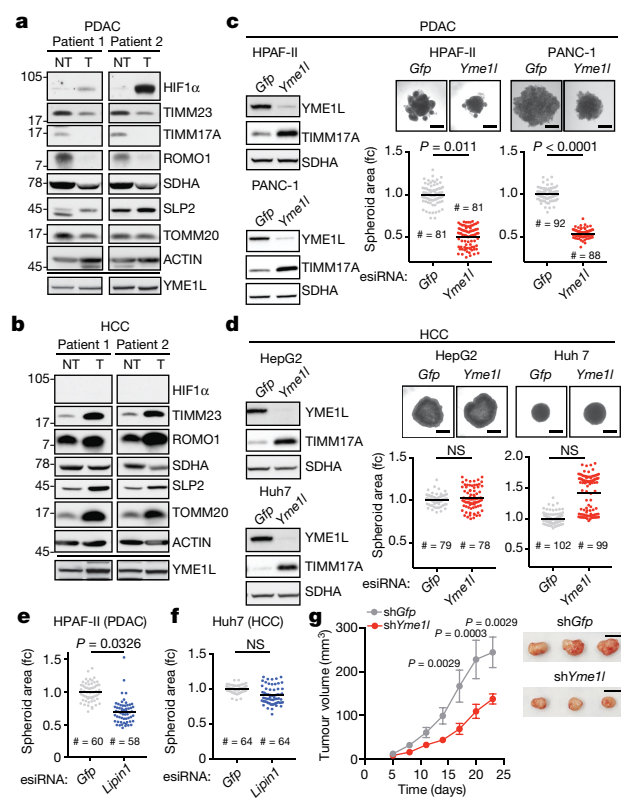


Fig. 4 | YME1L-mediated proteolysis is required for PDAC cell growth.

a, b, Immunoblot analysis of tumour (T) and corresponding adjacent non-tumour (NT) tissue lysates from patients with PDAC (**a**) or hepatocellular carcinoma (HCC) (**b**) ($n = 6$ independent patient samples; immunoblots from other patients are shown in Extended Data Fig. 9a, b). **c, d**, Spheroid surface areas of cancer cell lines treated with esiRNA targeting *Gfp* or *Yme1l*. **c**, HPAF-II and PANC-1; **d**, HepG2 and Huh7, all after 6 days. $n = 3$ (HPAF-II, HepG2), $n = 4$ (PANC-1, Huh7) independent experiments; # denotes number of spheroids. Immunoblots from $n = 1$ experiment. Scale bars, 0.5 mm; fc, fold change. **e, f**, Spheroid surface area of HPAF-II (**e**) and Huh7 (**f**) cells treated with esiRNA targeting *Gfp* or *Lipin1* after 6 days ($n = 4$ independent experiments). **g**, Xenograft growth of HPAF-II cells expressing sh*Gfp* or sh*Yme1l* in nude mice (sh*Gfp* $n = 10$ mice (day 5–20), $n = 9$ mice (day 20), $n = 7$ mice (day 23); sh*Yme1l* $n = 9$ mice; scale bars, 1 cm). x-axis shows days after injection of HPAF-II cells. Means \pm s.e.m.; two-tailed *t*-test (**c–f**), multiple *t*-test with assumption of same scatter within each population at each time point (**g**). NS, not significant.

metabolism, and examined the accumulation of YME1L substrates (Extended Data Fig. 8a). Only knockdown of the phosphatidic acid (PA) phosphatase LIPIN1 impaired YME1L-dependent proteolysis in Torin1-treated cells (Fig. 3f, Extended Data Fig. 8b–e). mTORC1-mediated phosphorylation of LIPIN1 inactivates its phosphatase activity, resulting in accumulation of PA and increased synthesis of glycerophospholipids^{23–25}. Mitochondrial PE levels were reduced upon inhibition of mTORC1 but maintained after depletion of LIPIN1 (Fig. 3g), demonstrating that LIPIN1 regulates accumulation of PE in mitochondria in response to mTORC1.

LIPIN1 limits the cellular accumulation of PA, which drives the membrane association and activation of CCT α , the rate-limiting enzyme for the synthesis of phosphatidylcholine (PC)^{26,27}. Whereas downregulation of LIPIN1 stabilized the YME1L substrate TIMM17A in Torin1-treated cells, additional depletion of CCT α in these cells restored proteolysis of TIMM17A (Fig. 3h, Extended Data Fig. 8e). The stability of TIMM17A mirrored mitochondrial PE levels (Fig. 3i): whereas depletion of LIPIN1 preserved PE in Torin1-treated cells, concomitant downregulation of CCT α blunted this effect and caused a decrease in mitochondrial PE (Fig. 3i). Thus, CCT α acts downstream of LIPIN1 to regulate proteolysis

by YME1L. Together, these results show that mTORC1 modulates mitochondrial PE via a phospholipid signalling cascade (Extended Data Fig. 8f): inhibition of mTORC1 activates LIPIN1, which decreases PA levels and CCT α -dependent formation of PC, ultimately limiting transport of PS to mitochondria and synthesis of PE by PISD.

We assessed spheroid growth of wild-type and *YME1L*^{-/-} cells upon downregulation of LIPIN1. Similar to YME1L deficiency (Extended Data Fig. 1a), depletion of LIPIN1 in wild-type cells impaired spheroid growth, whereas the poor growth of *YME1L*^{-/-} spheroids was unaltered by LIPIN1 depletion (Fig. 3j). Although other LIPIN1 paralogues may exert overlapping functions²⁸, this highlights the key role of the mTORC1–LIPIN1–YME1L signalling axis in reshaping the mitochondrial proteome and facilitating cellular adaptation to hypoxic growth conditions in spheroids.

YME1L promotes PDAC growth

PDACs are hypoxic, nutrient-deprived solid tumours²⁹ that adapt to their harsh microenvironment via a number of mechanisms, including rewiring glutamine metabolism³⁰. We therefore investigated whether stimulated YME1L-dependent proteolysis occurs in human PDACs by immunoblotting the lysates of tumour and non-tumour biopsy samples from six patients. Five out of the six individual tumours contained stabilized HIF1 α and YME1L substrates were strongly reduced in tumours compared to adjacent non-tumour tissue. Other mitochondrial proteins were mildly reduced in PDAC tumour tissue, indicating diminished mitochondrial biogenesis or enhanced mitophagy (Fig. 4a, Extended Data Fig. 9a). A similar analysis of hepatocellular carcinoma tumour samples taken from six individuals did not reveal HIF1 α stabilization or reduced levels of YME1L substrates (Fig. 4b, Extended Data Fig. 9b). Thus, YME1L-mediated proteolysis downstream of stabilization of HIF1 α may support tumour development in PDACs. Consistently, treatment of the PDAC cell lines HPAF-II and PANC-1 with *Yme1l*esiRNA significantly reduced the size and ATP content of spheroids (Fig. 4c, Extended Data Fig. 9c). Conversely, depletion of YME1L in two hepatocellular carcinoma cell lines, HepG2 and Huh7, had no negative effect on spheroid growth (Fig. 4d, Extended Data Fig. 9c). Downregulation of LIPIN1 also suppressed spheroid growth in HPAF-II cells, while having only a modest effect in Huh7 cells (Fig. 4e, f, Extended Data Fig. 9d, e). These results indicate that the LIPIN1–YME1L proteolytic axis facilitates PDAC growth but is dispensable for hepatocellular carcinoma progression. Finally, we stably suppressed YME1L in HPAF-II cells using short-hairpin RNA and monitored growth of these cells as xenografts in adult mice. Consistent with the spheroid data, depletion of YME1L strongly impaired PDAC tumour growth (Fig. 4g, Extended Data Fig. 9f, g). Collectively, these data highlight YME1L-mediated reshaping of the mitochondrial proteome as a mechanism that supports PDAC development and identify YME1L as a potential target in the treatment of PDAC.

Online content

Any methods, additional references, Nature Research reporting summaries, source data, extended data, supplementary information, acknowledgements, peer review information; details of author contributions and competing interests; and statements of data and code availability are available at <https://doi.org/10.1038/s41586-019-1738-6>.

- Porporato, P. E., Filigheddu, N., Pedro, J. M. B., Kroemer, G. & Galluzzi, L. Mitochondrial metabolism and cancer. *Cell Res.* **28**, 265–280 (2018).
- Mehta, M. M., Weinberg, S. E. & Chandel, N. S. Mitochondrial control of immunity: beyond ATP. *Nat. Rev. Immunol.* **17**, 608–620 (2017).
- Zhang, H., Menzies, K. J. & Auwerx, J. The role of mitochondria in stem cell fate and aging. *Development* **145**, dev143420 (2018).
- Mishra, P. & Chan, D. C. Metabolic regulation of mitochondrial dynamics. *J. Cell Biol.* **212**, 379–387 (2016).
- Mishra, P., Carelli, V., Manfredi, G. & Chan, D. C. Proteolytic cleavage of Opa1 stimulates mitochondrial inner membrane fusion and couples fusion to oxidative phosphorylation. *Cell Metab.* **19**, 630–641 (2014).
- Wai, T. et al. Imbalanced OPA1 processing and mitochondrial fragmentation cause heart failure in mice. *Science* **350**, aad0116 (2015).
- Stiburek, L. et al. YME1L controls the accumulation of respiratory chain subunits and is required for apoptotic resistance, cristae morphogenesis, and cell proliferation. *Mol. Biol. Cell* **23**, 1010–1023 (2012).
- Anand, R. et al. The i-AAA protease YME1L and OMA1 cleave OPA1 to balance mitochondrial fusion and fission. *J. Cell Biol.* **204**, 919–929 (2014).
- Sprenger, H. G. et al. Loss of the mitochondrial i-AAA protease YME1L leads to ocular dysfunction and spinal axonopathy. *EMBO Mol. Med.* **11**, e9288 (2019).
- Jiang, L. et al. Reductive carboxylation supports redox homeostasis during anchorage-independent growth. *Nature* **532**, 255–258 (2016).
- Mizushima, N. et al. A protein conjugation system essential for autophagy. *Nature* **395**, 395–398 (1998).
- Rainbolt, T. K., Lebeau, J., Puchades, C. & Wiseman, R. L. Reciprocal degradation of YME1L and OMA1 adapts mitochondrial proteolytic activity during stress. *Cell Rep.* **14**, 2041–2049 (2016).
- González, A. & Hall, M. N. Nutrient sensing and TOR signaling in yeast and mammals. *EMBO J.* **36**, 397–408 (2017).
- Saxton, R. A. & Sabatini, D. M. mTOR signaling in growth, metabolism, and disease. *Cell* **169**, 361–371 (2017).
- Brugarolas, J. et al. Regulation of mTOR function in response to hypoxia by REDD1 and the TSC1/TSC2 tumor suppressor complex. *Genes Dev.* **18**, 2893–2904 (2004).
- Huang, J. & Manning, B. D. The TSC1-TSC2 complex: a molecular switchboard controlling cell growth. *Biochem. J.* **412**, 179–190 (2008).
- Cunningham, J. T. et al. mTOR controls mitochondrial oxidative function through a YY1–PGC-1 α transcriptional complex. *Nature* **450**, 736–740 (2007).
- Morita, M. et al. mTORC1 controls mitochondrial activity and biogenesis through 4E-BP-dependent translational regulation. *Cell Metab.* **18**, 698–711 (2013).
- Laplante, M. & Sabatini, D. M. An emerging role of mTOR in lipid biosynthesis. *Curr. Biol.* **19**, R1046–R1052 (2009).
- Aaltonen, M. J. et al. MICOS and phospholipid transfer by Ups2-Mdm35 organize membrane lipid synthesis in mitochondria. *J. Cell Biol.* **213**, 525–534 (2016).
- Tasseva, G. et al. Phosphatidylethanolamine deficiency in mammalian mitochondria impairs oxidative phosphorylation and alters mitochondrial morphology. *J. Biol. Chem.* **288**, 4158–4173 (2013).
- Wai, T. et al. The membrane scaffold SLP2 anchors a proteolytic hub in mitochondria containing PARL and the i-AAA protease YME1L. *EMBO Rep.* **17**, 1844–1856 (2016).
- Eaton, J. M., Mullins, G. R., Brindley, D. N. & Harris, T. E. Phosphorylation of lipin 1 and charge on the phosphatidic acid head group control its phosphatidic acid phosphatase activity and membrane association. *J. Biol. Chem.* **288**, 9933–9945 (2013).
- Huffman, T. A., Mothe-Satney, I. & Lawrence, J. C., Jr. Insulin-stimulated phosphorylation of lipin mediated by the mammalian target of rapamycin. *Proc. Natl. Acad. Sci. USA* **99**, 1047–1052 (2002).
- Peterson, T. R. et al. mTOR complex 1 regulates lipin 1 localization to control the SREBP pathway. *Cell* **146**, 408–420 (2011).
- Craddock, C. P., Adams, N., Bryant, F. M., Kurup, S. & Eastmond, P. J. PHOSPHATIDIC ACID PHOSPHOHYDROLASE regulates phosphatidylcholine biosynthesis in *Arabidopsis* by phosphatidic acid-mediated activation of CTP:PHOSPHOCHOLINE CYTIDYLTRANSFERASE activity. *Plant Cell* **27**, 1251–1264 (2015).
- Jacquemyn, J., Cascalho, A. & Goodchild, R. E. The ins and outs of endoplasmic reticulum-controlled lipid biosynthesis. *EMBO Rep.* **18**, 1905–1921 (2017).
- Zhang, P. & Reue, K. Lipin proteins and glycerolipid metabolism: Roles at the ER membrane and beyond. *Biochim. Biophys. Acta Biomembr.* **1859**, 1583–1595 (2017).
- Vaziri-Gohar, A., Zarei, M., Brody, J. R. & Winter, J. M. Metabolic dependencies in pancreatic cancer. *Front. Oncol.* **8**, 617 (2018).
- Son, J. et al. Glutamine supports pancreatic cancer growth through a KRAS-regulated metabolic pathway. *Nature* **496**, 101–105 (2013).

Publisher's note Springer Nature remains neutral with regard to jurisdictional claims in published maps and institutional affiliations.

© The Author(s), under exclusive licence to Springer Nature Limited 2019

Methods

Construction of plasmids

Complementary DNA (cDNA) encoding human YME1L, OPA1ΔC (splice variant 7, 88–406 amino acids (aa)) with a C-terminal Myc tag and TIMM17A with a C-terminal Myc tag were cloned into pcDNA5/FRT/TO (Invitrogen) or pIVEX2.3d (Roche). cDNA strands encoding human PRELID3B with an N-terminal hexahistidine tag and TRIAP1 were amplified from cDNA by PCR and cloned into a pETDuet-1 (Merck). Human YME1L ΔMTS (151–716 aa), codon-optimized for expression in *Escherichia coli*, was synthesized (ThermoFisher) and cloned into pIVEX2.3d (Roche). Human SOD2 and LIAS cDNA were cloned into pGEM4. For lentiviral expression, cDNA encoding human PRELID3B with a C-terminal Flag tag was cloned into the pLVX-Puro (Invitrogen). cDNA encoding mutant YME1L(E543Q) and PRELID3B(T57K) were generated by site-directed mutagenesis PCR.

Cell culture, transfection and RNA interference

HeLa, HEK293T, HEK293 Flp-In T-Rex (HEK293), HT29 and SW480 cells and MEFs were maintained in DMEM-GlutaMAX (Life Technologies) containing 4.5 g/l glucose supplemented with 1 mM sodium pyruvate (Gibco), 100 μM non-essential amino acids (Gibco) and 10% (v/v) fetal bovine serum (Biochrom). Cell lines were maintained at 37 °C and 5% CO₂ and were routinely tested for mycoplasma infections. Cell line sources are listed in Supplementary Table 9. PDAC and HCC cancer cell lines were authenticated by short tandem repeat profiling. Cell growth was monitored by trypan blue exclusion and cell counting using the Countess automated cell counter (Thermo). For hypoxia treatments, cells were maintained in the H35 Hypoxystation (Don Whitley). Transfections of cell lines with DNA expression vectors were conducted with GeneJuice (Novagen). Lipofectamine RNAiMax (Invitrogen) was used for transfection of esiRNA and siRNA. Where indicated, the following compounds were added to the medium: Torin1 (400 nM), rapamycin (200 nM) and cycloheximide (100 μg/ml).

Generation of knockout cell lines

HeLa cells lacking *PRELID3B* were generated using CRISPR–Cas9-mediated gene editing. In brief, gene-specific DNA fragments were synthesized, cloned into pX335 (Addgene), and transfected into cells. Single clones were picked by limiting dilution and mutations were confirmed by genomic sequencing. HEK293 and HeLa cells lacking *YME1L* have previously been described^{31,32}. *OMAI*^{−/−} HEK293 cells³³ were depleted of *YME1L* using CRISPR–Cas9 as described above. *Yme1l*^{−/−}, *Oma1*^{−/−} and *Yme1l*^{−/−}/*Oma1*^{−/−} MEFs were previously described⁸. *Raptor* and *Rictor* knockout MEFs were generated by treating inducible iRaptor and iRictor MEFs with 1 μM 4-hydroxytamoxifen (4-OHT) as previously described^{34,35}.

Generation of stable expression cell lines

HEK293 Flp-In T-Rex cells were transfected with pcDNA5-FRT-TO (encoding the gene of interest) and pOG44 to generate stable tetracycline-inducible cell lines. Hygromycin (100 μg/ml) was used for selection. Expression was induced by incubating cells overnight with tetracycline (0.1 μg/ml). For lentiviral infection, HEK293T cells were transiently transfected with pLVX-puro (containing gene of interest) for 48 h by Lenti-X Packaging Single Shots (VSV-G) (Takara). Virus-containing culture supernatants were collected and cleared through a 0.45-μm filter before being added to HeLa cells in the presence of 4 μg/ml Polybrene. Infected cells were selected for using puromycin (3 μg/ml). For stable expression of short-hairpin RNA (shRNA), HPAF-II cells were infected with MISSION lentiviral transduction particles (Sigma) expressing shRNA targeting *Gfp* or *Yme1l* and positive clones were selected after puromycin selection.

Spheroid growth assay and cell culture on soft agar

HEK293 and HeLa cells were plated in Nunclon Sphera ultra-low attachment 96-well plates (Thermo) at concentrations of 1×10^4 and 0.5×10^4 cells per well, respectively. HeLa cells required brief centrifugation after plating to facilitate spheroid formation. Spheroids were maintained at 37 °C and 5% CO₂ for 7 days and fresh medium was exchanged every 2 days. Spheroids were imaged using a brightfield microscope (4× objective; Nikon) and their area measured with ImageJ/Fiji. Soft agar assays were performed using 1% and 0.6% noble agar as previously described³⁶.

Respiration measurements

OCRs were measured with a Seahorse Extracellular Flux Analyzer XFe96 (Agilent). Cell culture microplates were coated with poly-L-lysine (0.1 mg/ml) before 4×10^4 HEK293 cells were plated in each well. The assay medium included DMEM supplemented with glucose (25 mM) and glutamine (2 mM) where indicated. Cells were washed twice with assay media (+/− glutamine) and incubated for 1 h in a 37 °C non-CO₂ incubator before starting the assay. The basal OCR was normalized for the amount of protein per well by Bradford assay.

The Seahorse XF Mito Fuel Flex Test was used to measure the dependence of cells on the oxidation of three major metabolic substrates (glucose/pyruvate, fatty acids and glutamine) according to the manufacturer's instructions. In brief, the test uses three pathway inhibitors: mitochondrial pyruvate carrier inhibitor UK5099 (2 μM), carnitine palmitoyltransferase 1A inhibitor etomoxir (4 μM) or the glutaminase inhibitor BPTES (3 μM). HEK293 cells were incubated for 1 h in Seahorse assay medium without sodium pyruvate before the following measurements. First, the baseline OCR was monitored after 24 min. Second, the inhibitor of the target pathway was injected and the target inhibitor OCR was monitored after 36 min. Third, the inhibitors of the 2 remaining alternative pathways were simultaneously injected and the all inhibitors OCR was monitored after 36 min. To measure glucose/pyruvate dependence, UK5099 was injected first followed by Etomoxir and BPTES. To measure glutamine dependence, BPTES was injected first followed by Etomoxir and UK5099. To measure fatty acid dependence, Etomoxir was injected first followed by UK5099 and BPTES. The dependency on each oxidation pathway was calculated using the following equation: dependency (%) = (baseline OCR – target inhibitor OCR)/(baseline OCR – all inhibitors OCR).

ATP and NAD/NADH measurements

For measurement of the cellular ATP content in spheroids, the CellTiter-Glo 3D Luminescent Cell Viability Assay (Promega) was used according to the manufacturer's instructions. NAD and NADH measurements were made using an NAD/NADH Colorimetric Assay Kit (Abcam) according to the manufacturer's instructions.

RNA sequencing

Total RNA was extracted from cells using NucleoSpin RNA (Macherey-Nagel). Libraries were prepared using the Illumina TruSeq mRNA stranded sample preparation Kit. Library preparation started with 1 μg total RNA. After poly-A selection (using poly-T oligo-attached magnetic beads), mRNA was purified and fragmented using divalent cations under elevated temperature. The RNA fragments underwent reverse transcription using random primers. This was followed by second-strand cDNA synthesis with DNA Polymerase I and Rnase H. After end repair and A-tailing, indexing adaptors were ligated. The products were then purified and amplified (14 PCR cycles) to create the final cDNA libraries. After library validation and quantification (Agilent tape station), equimolar amounts of library were pooled. The pool was quantified by using the Peqlab KAPA Library Quantification Kit and the Applied Biosystems 7900HT Sequence Detection System. The pool was sequenced with a paired-end 100-nt protocol on an Illumina NovaSeq6000 sequencer. For bioinformatic analysis, raw reads

were mapped to mm10 (Ensembl build 91) with HiSat version 2.1.0 (PMID:25751142). Transcript assembly was performed using StringTie version 1.3.4d (PMID:25690850) and differential gene expression analysis was done with Cufflinks version 2.2.1 (PMID:2238036).

SDS-PAGE and immunoblot analysis

Cultured cells were washed with cold PBS and lysed on ice with RIPA buffer (50 mM Tris/HCl pH 7.4, 150 mM NaCl, 1 mM EDTA, 1% (v/v) Triton X-100, 0.1% (w/v) SDS, 0.5% (w/v) Na-deoxycholate) containing protease inhibitor cocktail (Roche) and PhosSTOP (Roche) for 30 min. After centrifugation at 15,500 rpm for 10 min at 4 °C, supernatant fractions were collected and analysed by SDS-PAGE and immunoblotting.

Tumour tissue preparation

For the analysis of human cancer tissue, two different cancer entities were used: pancreatic cancer (PDAC) and liver cancer (HCC). Six samples each of PDAC and HCC resected tumour and their corresponding adjacent non-tumour tissues were collected from the University Hospital of Cologne. The use of this tumour cohort for biomarker analysis has been approved by the Institutional Ethics Committee of the University Hospital of Cologne and written informed consent was obtained from all patients. The clinical and pathological characterization of patients is presented in Supplementary Table 12. The paired tumour and corresponding non-tumour tissue samples were snap frozen before protein extraction. A small piece of each tissue (about 3 mm³) was sonicated with 900 µl SDS-lysis buffer including protease inhibitor cocktail before SDS-PAGE and immunoblotting.

Immunofluorescence

HeLa cells grown on glass coverslips were fixed with 3.7% (v/v) paraformaldehyde in PBS for 15 min, permeabilized by 0.1% (v/v) Triton X-100 for 5 min, and incubated with primary antibodies in PBS containing 2% (w/v) bovine serum albumin. After washing, the cells were incubated with Alexa Fluor conjugated secondary antibodies. After washing, coverslips were mounted onto slides using ProLong Gold (ThermoFisher) and imaged with a confocal fluorescence microscope (LSM710 META, Carl Zeiss).

[³⁵S]-Methionine labelling and immunoprecipitation

HEK293 cells were plated on poly-L-lysine coated dishes (0.1 mg/ml) before all labelling experiments. For TIMM17A synthesis analysis, cells were treated +/− Torin1 for 2 h before cells were washed twice and incubated in labelling medium (L-Met and L-Cys free DMEM (Sigma) and dialysed FBS) without [³⁵S]-Met (+/− Torin1) for 30 min. Labelling medium including 25 µCi/ml [³⁵S]-Met +/− Torin1 was then added for 10, 30 and 60 min. For pulse chase analysis of TIMM17A and STARD7, cells were washed twice and incubated in labelling medium containing 25 µCi/ml [³⁵S]-Met for 1 h. Cells were then washed and incubated in normal growth medium +/− Torin1 for 4 and 6 h. For cell collection, cells were washed and scraped into ice cold PBS and briefly centrifuged before cell pellets were frozen on dry ice. For immunoprecipitation, cell pellets were resuspended in lysis buffer (50 mM Tris/HCl, 150 mM NaCl, 0.5% (v/v) NP40) containing protease inhibitor cocktail (Roche) and lysed on ice for 30 min. After centrifugation at 15,500 rpm for 10 min at 4 °C, supernatant fractions were incubated for 2.5 h with TIMM17A or STARD7 antibodies followed by 2.5 h with protein-A Fast Flow (Amersham Biosciences) at 4 °C. After repeated washing steps, bound proteins were eluted with SDS sample buffer (50 mM Tris/HCl pH 6.8, 2% (w/v) SDS, 5% (v/v) glycerol, 0.002% (w/v) bromophenol blue) and analysed by SDS-PAGE and autoradiography.

Metabolomics

HEK293 and MEFs were plated in 6-well dishes one day before metabolite extraction. Cells were washed twice with ammonium carbonate (75 mM, pH 7.4) at room temperature (RT) before plates were frozen

with liquid N₂. Extraction was performed by incubating cells twice with −20 °C 40:40:20 acetonitrile:methanol:water. Insoluble material was discarded by centrifuging extracts at 13,000 rpm for 2 min. The supernatant was collected and stored at −20 °C before analysis. Non-targeted metabolomics analysis was performed by flow-injection analysis on an Agilent 6550 QTOF instrument in negative mode ionization. Experimental conditions and processing are similar to what has previously been described³⁷. TCA cycle intermediates were identified in the spectral features by accurate mass using an *m/z* tolerance of 0.001.

Isolation of mitochondria

Cells were washed in PBS and resuspended in homogenization buffer (220 mM mannitol, 70 mM sucrose, 5 mM HEPES/KOH pH 7.4, 1 mM EGTA) with complete protease inhibitor. Cell suspension was homogenized with a rotating Teflon potter (Potter S, Braun) at 1,000 rpm followed by differential centrifugation. The homogenate was centrifuged at 600g for 5 min at 4 °C to remove the debris and nucleus, and the resulting supernatant was centrifuged at 8,000g for 10 min at 4 °C to obtain mitochondrial fractions. For the phospholipid analysis, mitochondria were further purified by density gradient centrifugation: mitochondria were layered on top of a Percoll step gradient (12, 19, 40% Percoll in homogenization buffer) followed by ultracentrifugation (42,000g, 30 min, 4 °C) in SW41Ti rotor (Beckman). The mitochondrial fraction was isolated and washed with homogenization buffer.

Mitochondrial protein import assay

The radiolabelled precursor protein LIAS (lipoyl synthase) was synthesized for 1 h at 30 °C using the SP6 promoter TNT Quick Coupled Transcription/Translation System (Promega) containing 20 µCi [³⁵S]-methionine. Protein import was initiated by incubating precursor protein with crude mitochondria at 30 °C in the absence of protease inhibitor as previously described³¹. To abolish membrane potential, CCCP (1 mM) was included. Import was stopped by placing on ice and all samples were incubated with proteinase K (20 µg/ml) for 20 min to degrade non-imported precursor protein. Mitochondria were then washed in wash buffer (220 mM mannitol, 70 mM sucrose, 5 mM HEPES/KOH pH 7.4, 1 mM EGTA) containing PMSF (1 mM) and resuspended in SDS sample buffer and analysed by SDS-PAGE and autoradiography.

Isolated mitochondria proteomics in normoxia and hypoxia

In solution digestion of protein for mass spectrometry. Isolated mitochondria (50 µg) were lysed in RIPA buffer and 1 µl GlycoBlue was added for acetone precipitation overnight at −20 °C. The samples were centrifuged for 10 min at 15,000g at 4 °C and the pellet was washed with 90% acetone (−20 °C). Protein pellets were resuspended in 6 M urea/2 M thiourea in 10 mM HEPES. Proteins were reduced by adding DTT to a final concentration of 10 mM and incubation for 30 min at RT. Alkylation was performed using 55 mM iodoacetamide (20 min in the dark). Pre-digestion was performed by adding Lys-C (Wako) at an enzyme:substrate ratio of 1:100 and incubated at RT for 2–3 h. 50 mM ammonium bicarbonate was used to dilute the urea concentration to 2 M. Trypsin (Sigma Aldrich, T6567) was subsequently added at an enzyme:substrate ratio of 1:100. Digestion was performed overnight and stopped by acidification (1:1 (v/v) 5% acetonitrile, 1% TFA). Samples were primed using the STAGE tip technique³⁸ before LC-MS/MS analysis.

Liquid chromatography and tandem mass spectrometry (LC-MS/MS). Peptides were eluted from C18 tips using 0.1% formic acid in 60% acetonitrile (ACN), concentrated in a speed vac to complete dryness and re-suspended in 5% formic acid and 2% acetonitrile. The LC-MS/MS equipment consisted of an EASY nLC 1000 coupled to the quadrupole based QExactive Plus instrument (Thermo Scientific) via a nano-spray electroionization source. Peptides were separated on an in-house packed 50-cm column (1.9-µm C18 beads, Dr. Maisch) using a binary

Article

solvent buffer system: A) 0.1% formic acid and B) 0.1% formic acid in acetonitrile. The content of buffer B was raised from 7% to 23% within 220 min followed by an increase to 45% within 10 min. Then, within 5 min the buffer B fraction was raised to 80% and held for a further 5 min before being decreased to 5% within 5 min and held there for a further 5 min. Eluting peptides were ionized in positive mode by an applied voltage of 2.4 kV. The capillary temperature was 275 °C and the S-lens RF level was set to 64. The following settings were used: MS1-70,000 (at 200 *m/z* resolution, 3×10^6 AGC target, 20-ms maximum injection time, 300–1,750-Th scan range. In a data-dependent mode, the 10 most intense peaks were selected for isolation and fragmentation in the HCD cell using a normalized collision energy of 25 and an isolation window of 2.0 Th. Dynamic exclusion was enabled and set to 20 s. The MS/MS scan properties were: 17,500 (at 200 *m/z* resolution, 5×10^5 AGC target and a maximum injection time of 50 ms.

MaxQuant analysis and bioinformatics. Raw files were processed with MaxQuant³⁹ and Andromeda search engine⁴⁰. Recorded MS/MS spectra were compared to the mouse Uniprot reference proteome at mass tolerance of 7 ppm and 4.5 ppm for first and main searches, respectively. Oxidation at methionine residues and protein N-terminal acetylation were considered as variable modifications and carbamido-methylation at cysteine residues was defined as a fixed modification. Match-between-runs and label-free quantification were enabled using default settings. To identify proteins that were significantly differentially expressed, a two sided *t*-test was applied. Correction for multiple testing was performed by a permutation-based false discovery rate (FDR) calculation (# of perm.: 500, fudge factor $s_0 = 0.1$, FDR <0.05). Gene Ontology, KEGG, PFAM and GSEA annotations were matched based on Uniprot identifiers and 1D enrichment⁴¹ was carried out at a significance FDR level of 0.02 determined by Benjamini–Hochberg correction.

Potential YME1L substrates were identified and classified using the following criteria: (1) mitochondria associated function based on Gene Ontology Cellular Compartment (GOCC); (2) significant upregulation (FDR <0.05) in *Yme1l^{-/-}* cells compared to WT in normoxia or exclusively detected in *Yme1l^{-/-}* cells ($n \geq 3$) and not detected at all in WT cells; (3) Downregulation (log₂ ratio <−0.58) in WT cells in hypoxia compared to normoxic conditions or exclusively quantified ($n \geq 3$) in normoxia and not detected at all in hypoxia; and (4) no regulation (absolute log₂ ratio <0.58) between hypoxia and normoxia in *Yme1l^{-/-}* cells. Class I substrates meet all four criteria. Class II substrates meet only criteria 1 and 2. In the accompanying Supplementary Table 1, matching protein groups per criteria are annotated.

Visualization was done using InstantClue⁴². For visualization of identified potential substrates in a heat map (Fig. 1g), missing values were replaced by random values drawn from a downshifted Gaussian distribution (downshift: $1.8 \times$ s.d. of the median, width: $0.4 \times$ s.d.).

Proteomics of Torin1-treated or Gln/Leu-starved MEF cells

Protein digestion. Cell pellets were washed in PBS and resuspended in 40 μ l of heated (70 °C) 2% SDC (sodium deoxycholate, 30970, Sigma Aldrich) lysis buffer (100 mM Tris/HCl pH = 8.5) and incubated for 15 min at 90 °C. Samples were sonicated (Sonoplus mini20, MS 2.5 Sonotrode Bandelin) to disrupt cells and dissolve proteins. Lysates were cleared by centrifugation (10 min, 12,000g, RT). Protein concentration was determined using the 660 nm Protein Assay (Pierce, Thermo Fisher Scientific, 22660). Forty micrograms protein was reduced and alkylated for 45 min at 45 °C in the dark using 10 mM TCEP (646547, Sigma Aldrich) and 15 mM CAA (108448, Sigma Aldrich). One microgram of Lys-C (Wako) and Trypsin (Sigma Aldrich) was added and samples were incubated for 16 h at 37 °C. Samples were acidified by adding 10% TFA to a final concentration of 2%. Precipitated SDC was removed by centrifugation (15 min, 12,000g, RT) and peptides were desalting using the StageTip (material: SDB-RPS, Affinisept) technique.

To generate the peptide spectral library, 1 mg of pooled samples (all conditions pooled 1:1) was digested as described above. Desalting was performed using SepPak 50 mg Cartridges (Waters) and peptides were separated using a Dionex 3000 chromatography system. The buffer systems consisted out of two buffers. A) 10 mM ammonium hydroxide and B) 90% acetonitrile and 10 mM ammonium hydroxide. Peptides were separated according to their hydrophobicity using a Waters XBridge BEH C18 130 Å (length = 250 mm, inner diameter = 3 mm, 3.5- μ m beads) column. The gradient length was 60 min and in total, 40 fractions were collected (1/60 s) and subsequently concentrated using a speed vac. Peptides were dissolved in 40 μ l 2% formic acid, 2.5% acetonitrile. For LC–MS/MS measurement, 2 μ g peptides per fraction were injected.

LC–MS/MS. LC–MS/MS instrumentation consisted out of an Easy nLC-1200 (Thermo Fisher) coupled via a nanospray ionization source to a QExactive HF-x (Thermo Fisher) mass spectrometer. Liquid chromatography gradients were identical for MS/MS spectra library and data-independent acquisition (DIA) measurements using two different solvents A and B (buffer A: 0.1% formic acid and buffer B: 0.1% formic acid in 80% acetonitrile). The in-house packed column length was 45 cm and the inner diameter was 75 μ m. The column was filled with PoroShell C18 2.7- μ m (Agilent Technologies) beads and was kept in a column oven at 50 °C (PRSO-V2, Sonation). The buffer B percentage was linearly raised from 5% to 29% within 30 min and further increased to 55% within 7 min. The column was washed at 95% B for 7 min. All samples were measured in random order.

MS/MS library—data dependent acquisition. For the MS/MS spectra library, the QExactive HF-x operated in a Top22 data-dependent mode. MS1 spectra were acquired in a mass range of 350–1,750 *m/z*, using an AGC target of 3×10^6 and a resolution at 200 *m/z* of 60,000. MS/MS spectra were acquired at 15,000 resolution using an AGC target of 5×10^5 and a maximal injection time of 22 ms.

DIA. For DIA measurements, MS1 spectra were acquired using a resolution of 60,000 and an AGC target of 1×10^6 . For MS/MS independent spectra acquisition, 48 windows were acquired at an isolation *m/z* range of 15 Th and the isolation windows overlapped by 1 Th. The isolation centre range covered a mass range of 385–1,043 *m/z*. Fragmentation spectra were acquired at a resolution of 15,000 at 200 *m/z* using a maximal injection time of 22 ms and stepped normalized collision energies (NCE) of 24, 27, 30. The default charge state was set to 4.

Bioinformatics and data analysis. To generate the MS/MS spectra library, acquired raw files were analysed by MaxQuant (1.5.3.8) and the implemented Andromeda search engine using default settings. MS/MS spectra were correlated against the Uniprot mouse reference proteome (June 2018). The FDR was controlled by the implemented decoy algorithm and set to 1% at the peptide-spectrum match and protein level. Evidence.txt and msms.txt output files were loaded into Spectronaut 13 containing 173,464 identified peptide sequences (10,520 protein groups). Acquired DIA raw files were analysed by Spectronaut 13 (Biognosis) using default settings (*q* value <0.01). Experiments (Torin1 treatment, glutamine and leucine starvation) were analysed separately. Search smc files can be opened and viewed with Spectronaut Viewer and are publicly available via the PRIDE partner repository (<https://www.ebi.ac.uk/pride/archive/projects/PXD011750>; <https://www.ebi.ac.uk/pride/archive/projects/PXD014405>). Missing values were replaced using randomly drawing values from a down-shifted Gaussian distribution. Visualization was performed using InstantClue.

Quantitative mass spectrometry of phospholipids

Mass spectrometric analysis was performed essentially as previously described⁴³. Lipids were extracted from 10 μ g proteins of isolated mitochondria in the presence of internal standards of major phospholipids

(PC 17:0–20:4, PE 17:0–20:4, PI 17:0–20:4, PS 17:0–20:4, PG 17:0–20:4, PA 17:0–20:4, all from Avanti Polar Lipids) and CL (CL mix I, Avanti Polar Lipids). Extraction was performed as previously described⁴⁴. Lipids were dissolved in 10 mM ammonium acetate in methanol, and analysed on a QTRAP 6500 triple quadrupole mass spectrometer (SCIEX) equipped with nano-infusion splay device (TriVersa NanoMate with ESI-Chip type A, Advion) under following settings: (QT6500) CUR, 20; CAD, medium; IHT, 90 °C; EP, 10; Mode: Highmass; Step size, 0.1 Da; Setting time, 0 ms; Scan rate, 200 Da/s; Pause 5 ms; CEM, 2300; Sync, LC sync; Ccan mode, Profile (NanoMate) sample infusion volume, 12 µl; volume of air to aspirate after sample, 1 µl; air gap before chip, enabled; aspiration delay, 0 s; pre-piercing, with Mandrel; spray sensing, enabled; temperature, 12 °C; gas pressure, 0.4 psi; ionization voltage, 1.15 kV; polarity, positive; vent headspace, enabled; pre-wetting, 1×; volume after delivery, 0.5 µl; contact closure delay, 1 s; volume timing delay, 0 s; aspiration depth, 1 mm; pre-piercing depth, 9 mm; output contact closure, Rel 1/2.5 s duration. The quadrupoles Q1 and Q3 were operated at unit resolution. PC analysis was carried out in positive ion mode by scanning for precursors of *m/z* 184 at a collision energy (CE) of 50 eV. PE, PI, PS, PG and PA measurements were performed in positive ion mode by scanning for neutral losses of 141 Da, 277 Da, 185 Da, 189 Da and 115 Da at CEs of 25 eV, 30 eV, 20 eV, 30 eV and 25 eV, respectively. CL species were identified in positive ion mode by scanning for precursors of the masses (*m/z* 465.4, 467.4, 491.4, 493.4, 495.4, 505.5, 519.5, 521.5, 523.5, 535.5, 547.5, 549.5, 551.5, 573.5, 575.5, 577.5, 579.5, 601.5, 603.5, 605.5, 607.5, 631.5, 715.5 and 771.5 Da) of corresponding DAG-H₂O fragments as singly charged ions at CEs of 40–50 eV. Mass spectra were processed by the LipidView Software Version 1.2 (SCIEX) for identification and quantification of lipids. Lipid amounts (pmol) were corrected for response differences between internal standards and endogenous lipids. Correction of isotopic overlap in CL species was performed as previously described⁴³.

Expression in *E. coli* and purification of human TRIAP1

N-terminally His7-TCS (TEV Cleavage Site)-tagged human TRIAP1 was expressed in *E. coli* Origami B (DE3) (Promega). After incubation at 37 °C for 2.5 h (OD₆₀₀ about 0.5), the culture was shifted to 24 °C for 1 h and then His7TCS-hTRIAP1 was expressed by adding IPTG (0.1 mM) for 5 h. *E. coli* cells were lysed in buffer B (50 mM Tris/HCl pH 8, 250 mM NaCl, 1× complete protease inhibitor mix, 1 mM PMSF, 100 U/ml DNaseI, 1 mM MgCl₂) containing 20 mM imidazole. The lysate was spun at 30,000g for 20 min and the supernatant was recovered to a tube. The supernatant was applied to a His-Trap HP column (1 ml, GE healthcare). After washing the column with 5 column volumes of buffer B containing 40 mM imidazole, His-tagged proteins were eluted by 12 ml linear gradient of imidazole (up to 500 mM) in buffer B. Peak fractions were collected and concentrated to 0.5 ml in an Amicon-4 centrifuge unit. The concentrate was subjected to size-exclusion chromatography using Superdex 75 10/300 GL column (GE healthcare) in buffer C (10 mM Tris/HCl pH 8.0, 500 mM NaCl). Peak fractions were collected and concentrated to 0.5 ml in an Amicon-4 centrifuge unit. After dialysis in dialysis buffer (10 mM Tris/HCl pH 7.4, 150 mM NaCl), protein concentration in the sample was determined by absorbance at 280 nm. Two milligrams protein was treated in 1 ml of TEV reaction mix (50 mM Tris/HCl pH 8.0, 0.1 mM EDTA, 3 mM GSH, 0.3 mM GSSG, 0.2 U/µl AcTEV (Invitrogen)) for 24 h at 16 °C. Samples were diluted in 4 ml buffer B containing 20 mM imidazole and subjected to His-TRAP purification to remove AcTEV and uncleaved proteins (both carry a polyhistidine tag). The flow through fraction was collected, and concentrated to 0.5 ml in an Amicon-4 centrifuge unit. The concentrate was subjected to size-exclusion chromatography using Superdex 75 10/300 GL column (GE healthcare) in buffer C (10 mM Tris/HCl pH 8.0, 500 mM NaCl). Peak fractions were collected, and concentrated to 0.2 ml in an Amicon-4 centrifuge unit. After dialysis in dialysis buffer (10 mM Tris-HCl, pH 7.4, 150 mM NaCl), protein concentration in the sample was determined

by absorbance at 280 nm. Samples were divided into small aliquots and then stored at –80 °C.

Synthesis in cell-free expression system and purification of PRELID3B-TRIAP1

N-terminally His-tagged PRELID3B together with TRIAP1 were expressed in a bacterial lysate-based, continuous-exchange cell-free expression system as previously described in detail⁴⁵ using pETDuet-hisPRELID3B-TRIAP1 or the variant thereof encoding PRELID3B^{T57K} mutants. Protein expression was achieved by shaking at 30 °C for 16 h in S30 lysate of *E. coli* with T7 polymerase (Cube Biotech, 35% (v/v) in reaction mix) supplemented with 100 mM HEPES/KOH pH 8.0, 20 mM EDTA, 10 mM Tris-acetate (pH 8.2), 16 mM Mg(OAc)₂, 160 mM KOAc, 1.55 mM RCWMDE (arginine, cysteine, tryptophan, methionine, aspartic acid and glutamic acid), 0.55 mM other essential amino acids, 20 mM lithium potassium acetyl phosphate (AcP), 20 mM phosphoenolpyruvic acid (PEP), 1.5 mM ATP, 1 mM CTP, 1 mM GTP, 1 mM UTP, 0.1 mg/ml folic acid, 2% (w/v) PEG8000, 0.05% sodium azide, 0.5 mg/ml tRNA, 0.3 U/µl RNasin, 40 µg/ml pyruvate kinase, 1× complete protease inhibitor cocktail, 10 µM purified hTRIAP1 and 15 µg/ml plasmid DNA (all end concentrations). Insoluble material was removed by centrifugation (20 min, 16,000g, 4 °C). The supernatant was recovered to a new tube and diluted in 10× volume of binding buffer B (50 mM Tris/HCl pH 8.0, 250 mM NaCl, 20 mM imidazole, 1× complete EDTA, 1 mM PMSF). Ni-sepharose high-performance beads (GE healthcare) were added to the suspension (20 µl per ml) and His-tagged proteins were captured to beads by incubation for 1 h at 4 °C. After incubation, beads were recovered by centrifugation (1,000g, 2 min), washed four times with 50× beads volume of wash buffer B (20 mM Tris/HCl pH 8.0, 250 mM NaCl, 30 mM imidazole) and then proteins were eluted in elution buffer B (20 mM Tris/HCl pH 8.0, 250 mM NaCl, 300 mM imidazole). The elution was subjected to dialysis in storage buffer (10 mM Tris/HCl pH 7.4, 100 mM NaCl, 1 mM EDTA) for 4 h. Protein concentration in samples was determined by absorbance at 280 nm with extinction coefficient of the protein complex. The samples were used for lipid transfer assay immediately.

Lipid transfer assays

Lipid transfer of NBD-PS by PRELID3B-TRIAP1 was performed as previously described^{20,46}. Unless otherwise indicated in legends, lipid transfer activities were tested in the assay buffer (20 mM Tris/HCl pH 7.4, 100 mM NaCl, 1 mM EDTA) at 20 °C. To assess PS transfer by PRELID3B-TRIAP1, donor liposomes (12.5 µM; DOPC/DOPE/CL/Lac-PE/NBD-PS/Rhod-PE = 50/23/15/5/2%) and acceptor liposomes (50 µM; DOPC/DOPE/CL/Lac-PE/DOPS = 50/25/15/5%) were incubated with lipid transfer proteins (typically 400 nM) for 5 min. We monitored dequenching of NBD-labelled phospholipids upon transfer to acceptor liposomes and normalized NBD fluorescence to liposomes lacking the quencher Rhodamine-PE as 100%. Molecules of NBD-PS transported per complex and second were calculated from the alteration in NBD fluorescence within the initial 30 s.

Reconstitution of YME1L and substrates into liposomes for monitoring YME1L activity

YME1L^{AMTS} and OPA1^{ΔC} or TIMM17A were expressed in the cell-free expression system, as described above, using pIVEX2.3d expression vectors in the presence of mitochondrial inner membrane mimicked liposomes (25 mM; DOPC/DOPE/CL/Soy-PI/DOPS/Rhod-PE = 40/34/18/5/3/0.01%) at 30 °C for 3 h. For liposome preparation, phospholipids (10 mM DOPC, 8.5 mM DOPE, 4.5 mM CL, 0.75 mM DOPS, 1.25 mM Soy-PI, and 0.01 mM Rhod-PE) were mixed and chloroform was evaporated under nitrogen flow at 37 °C. Liposomes were dissolved in buffer (5 mM Tris/HCl pH 8.5, 10 mM KOAc) by vortexing, and extruded with a mini extruder and a polycarbonate membrane (Avanti polar lipids, 0.1 µm) according to the manufacturer's protocol. When the

concentration of PE in liposomes was increased or decreased, the concentration of PC was adjusted accordingly. Liposomes with incorporated proteins were collected by centrifugation (20 min, 16,000g, 4 °C) and soluble proteoliposomes were separated by a 40, 30, 15, and 0% sucrose gradient centrifugation (200,000g, 1.5 h, 4 °C). Collected soluble proteoliposomes on the top fraction were incubated in reaction buffer (10 mM Tris/HCl (pH 7.4), 50 mM NaCl, 4 mM ATP (pH7), 8 mM Mg(OAc)₂, 50 µM Zn(OAc)₂, 2 mM DTT) at 37 °C for the indicated times. Samples were separated by SDS-PAGE and substrates were detected by immunoblotting.

Mouse xenograft model

Mouse experiments were conducted according to protocols approved by the responsible national and local authority (81-02.04.2018.A139; LANUV NRW). Three million *Gfp* shRNA or *YmeII* shRNA HPAF-II cells were resuspended in 100 µl DMEM without FBS and subcutaneously injected into 6-week-old female Balb/c nude mice (Janvier Labs) on the left flank. Tumour size was measured with calipers every 3 days and tumour volume was calculated using the formula $1/2(\text{length} \times \text{width}^2)$. After 4 weeks of xenograft injection, mice were euthanized and xenograft tumours were collected for further analysis. Three mice were euthanized at earlier time points owing to the presence of open wounds in the tumours. No tumours reached the approved protocol size limit of 1.5 cm. Mice were randomly distributed into experimental groups and mouse numbers were determined on the basis of previous experience.

Statistical analyses

The statistical significance was assessed using two-tailed *t*-test or one-way or two-way ANOVAs as indicated. All reported *n* numbers refer to biological replicates. A *P* value of <0.05 was considered statistically significant.

Reporting summary

Further information on research design is available in the Nature Research Reporting Summary linked to this paper.

Data availability

The mass spectrometry proteomics data have been deposited to the ProteomeXchange Consortium via the PRIDE partner repository with the following dataset identifiers: PXD011750 (DDA data—hypoxia/normoxia WT and *YmeII*^{-/-} MEF mitochondria, <https://www.ebi.ac.uk/pride/archive/projects/PXD011750>) and PXD014405 (MEF MS/MS library and DIA data, <https://www.ebi.ac.uk/pride/archive/projects/PXD014405>). Transcriptomic data from hypoxia/normoxia WT MEF cells have been deposited to the GEO omnibus (accession number GSE133753). These datasets are presented in Supplementary Tables 1–6. Uncropped immunoblot images are available in Supplementary Fig. 1 and all Source Data are available online.

31. Saita, S. et al. PPAR partitions the lipid transfer protein STARD7 between the cytosol and mitochondria. *EMBO J.* **37**, e97909 (2018).
32. Hartmann, B. et al. Homozygous YMEII mutation causes mitochondrialopathy with optic atrophy and mitochondrial network fragmentation. *eLife* **5**, e16078 (2016).
33. Baker, M. J. et al. Stress-induced OMA1 activation and autocatalytic turnover regulate OPA1-dependent mitochondrial dynamics. *EMBO J.* **33**, 578–593 (2014).
34. Cybulski, N., Zinzalla, V. & Hall, M. N. Inducible raptor and rictor knockout mouse embryonic fibroblasts. *Methods Mol. Biol.* **821**, 267–278 (2012).
35. Robitaille, A. M. et al. Quantitative phosphoproteomics reveal mTORC1 activates de novo pyrimidine synthesis. *Science* **339**, 1320–1323 (2013).
36. Borowicz, S. et al. The soft agar colony formation assay. *J. Vis. Exp.* e51998 (2014).
37. Fuhrer, T., Heer, D., Begemann, B. & Zamboni, N. High-throughput, accurate mass metabolome profiling of cellular extracts by flow injection-time-of-flight mass spectrometry. *Anal. Chem.* **83**, 7074–7080 (2011).
38. Rappaport, J., Ishihama, Y. & Mann, M. Stop and go extraction tips for matrix-assisted laser desorption/ionization, nanoelectrospray, and LC/MS sample pretreatment in proteomics. *Anal. Chem.* **75**, 663–670 (2003).
39. Cox, J. & Mann, M. MaxQuant enables high peptide identification rates, individualized p.p.b.-range mass accuracies and proteome-wide protein quantification. *Nat. Biotechnol.* **26**, 1367–1372 (2008).
40. Cox, J. et al. Andromeda: a peptide search engine integrated into the MaxQuant environment. *J. Proteome Res.* **10**, 1794–1805 (2011).
41. Cox, J. & Mann, M. 1D and 2D annotation enrichment: a statistical method integrating quantitative proteomics with complementary high-throughput data. *BMC Bioinformatics* **13** (Suppl. 16), S12 (2012).
42. Nolte, H., MacIver, T. D., Tellkamp, F. & Krüger, M. Instant Clue: a software suite for interactive data visualization and analysis. *Sci. Rep.* **8**, 12648 (2018).
43. Tatsuta, T. Quantitative analysis of glycerophospholipids in mitochondria by mass spectrometry. *Methods Mol. Biol.* **1567**, 79–103 (2017).
44. Bligh, E. G. & Dyer, W. J. A rapid method of total lipid extraction and purification. *Can. J. Biochem. Physiol.* **8**, 911–917 (1959).
45. Schwarz, D. et al. Preparative scale expression of membrane proteins in *Escherichia coli*-based continuous exchange cell-free systems. *Nat. Protocols* **2**, 2945–2957 (2007).
46. Potting, C. et al. TRIAP1/PRELI complexes prevent apoptosis by mediating intramitochondrial transport of phosphatidic acid. *Cell Metab.* **18**, 287–295 (2013).
47. Titov, D. V. et al. Complementation of mitochondrial electron transport chain by manipulation of the NAD⁺/NADH ratio. *Science* **352**, 231–235 (2016).
48. Scheuner, D. et al. Translational control is required for the unfolded protein response and *in vivo* glucose homeostasis. *Mol. Cell* **7**, 1165–1176 (2001).
49. Thoreen, C. C. et al. A unifying model for mTORC1-mediated regulation of mRNA translation. *Nature* **485**, 109–113 (2012).

Acknowledgements We thank D. Ehrentraut for expert technical assistance; L. Raatz and M. Heitmann for assisting with xenograft analysis and tissue protein extraction; and A. Wilbrandt-Hennes and U. Cullmann of the CECAD proteomics facility for technical assistance. RNA sequencing was performed at the Cologne Center for Genomics and Data Analysis in the MPI Biology of Ageing bioinformatics core facility. We thank J. Altmüller, M. Franitzka, F. Metge and J. Boucas for technical and bioinformatic assistance. This work was supported by grants from the Deutsche Forschungsgemeinschaft (La918/15-1; SFB1218/A1), the German-Israeli-Project (DIP; RA1028/10-1) and the Max-Planck-Society to T.L.; EMBO and Alexander von Humboldt fellowships to T.M. (GA-2013-609409, ALTF 1220-2014); and a fellowship of the Japan Society for the Promotion of Science (JSPS) for research abroad, The Osamu Hayashi Memorial Scholarship for Study Abroad and grants from the Uehara Memorial Foundation to Y.O. We are grateful for the following gifts: *Tsc2*^{-/-} MEFs from C. Demetriades and D. Kwiatkowski, *Atg5*^{-/-} MEFs from K. Winklhofer, WT (S/S) and EIF2 α ^{SS1A} knock-in MEFs from R. Kaufman, 4E-BP DKO, iRaptor and iRictor MEFs from H. McBride and pUC57-LbNOX from V. Mootha (Addgene plasmid # 75285).

Author contributions The study was conceived and designed by T.M., Y.O. and T.L.; T.M. performed the analysis in hypoxia and spheroids; Y.O. performed lipid analysis and *in vitro* reconstitution experiments; proteomic experiments were performed and evaluated by T.M., B.L., F.C.M., H.N. and M.K.; metabolomic experiments were performed by T.M. and N.Z.; T.T. performed lipid transfer assays; H.-G.S. supported data interpretation; Y.Z., J.L. and C.B. provided support for clinical materials and performed the xenograft assay; T.M., M.H. and J.R. performed and evaluated import and labelling experiments; R.S., M.P., S.H. and J.C.B. assisted with *in vivo* studies and supported data interpretation; T.M., Y.O. and T.L. wrote the manuscript, which was edited by all authors.

Competing interests The authors declare no competing interests.

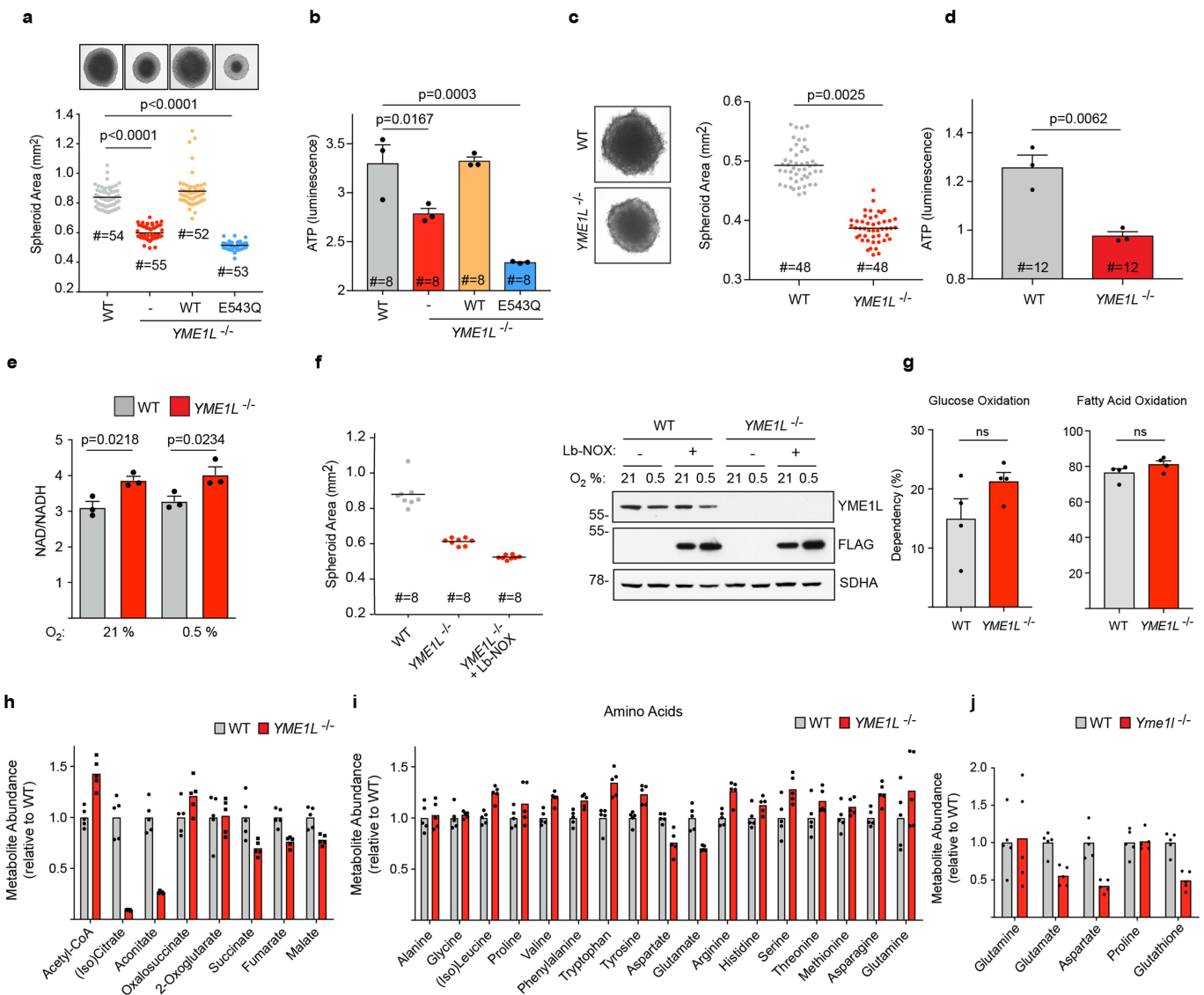
Additional information

Supplementary information is available for this paper at <https://doi.org/10.1038/s41586-019-1738-6>.

Correspondence and requests for materials should be addressed to T.L.

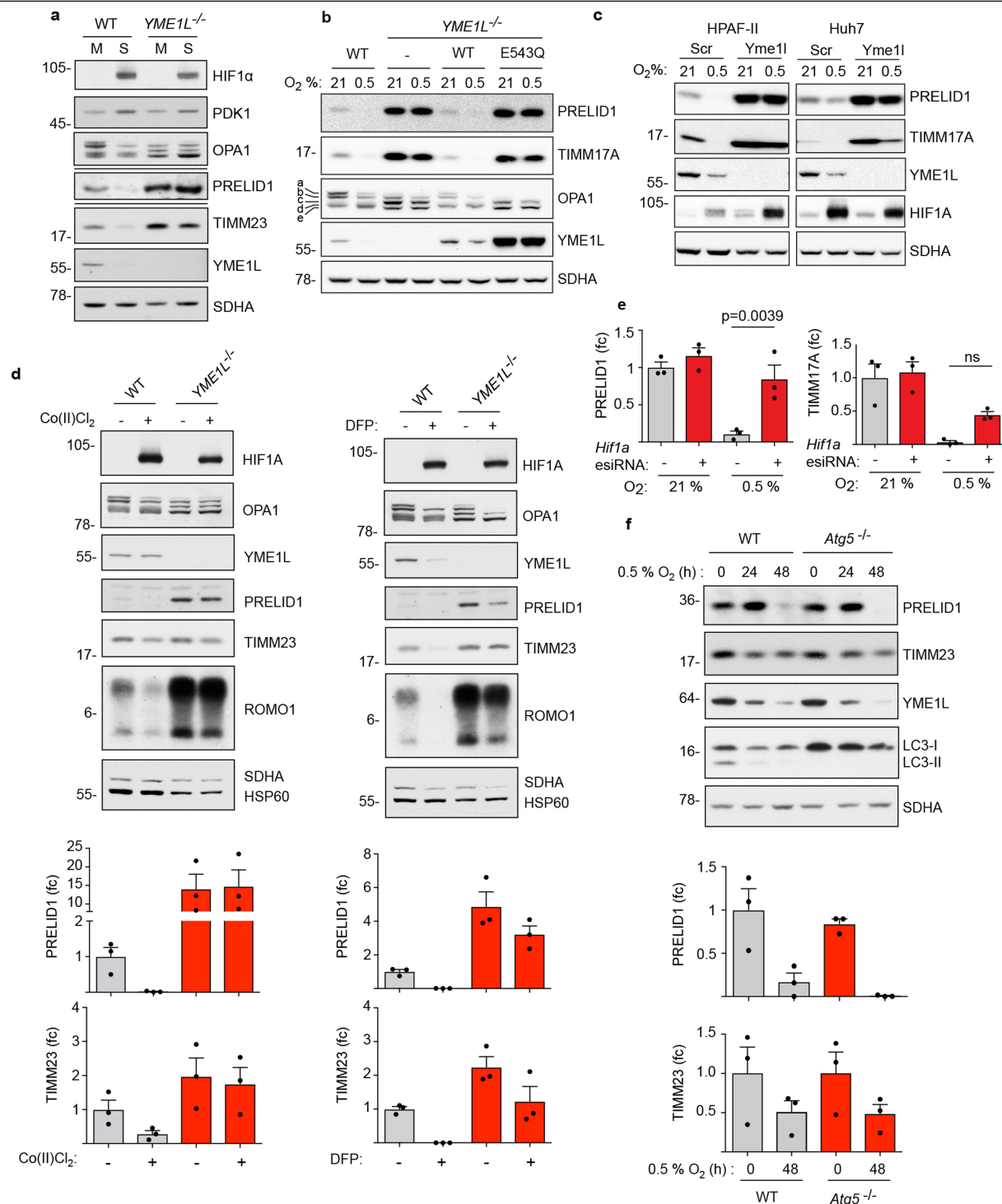
Peer review information *Nature* thanks Thomas Becker, Markus Ralser and the other, anonymous, reviewer(s) for their contribution to the peer review of this work.

Reprints and permissions information is available at <http://www.nature.com/reprints>.



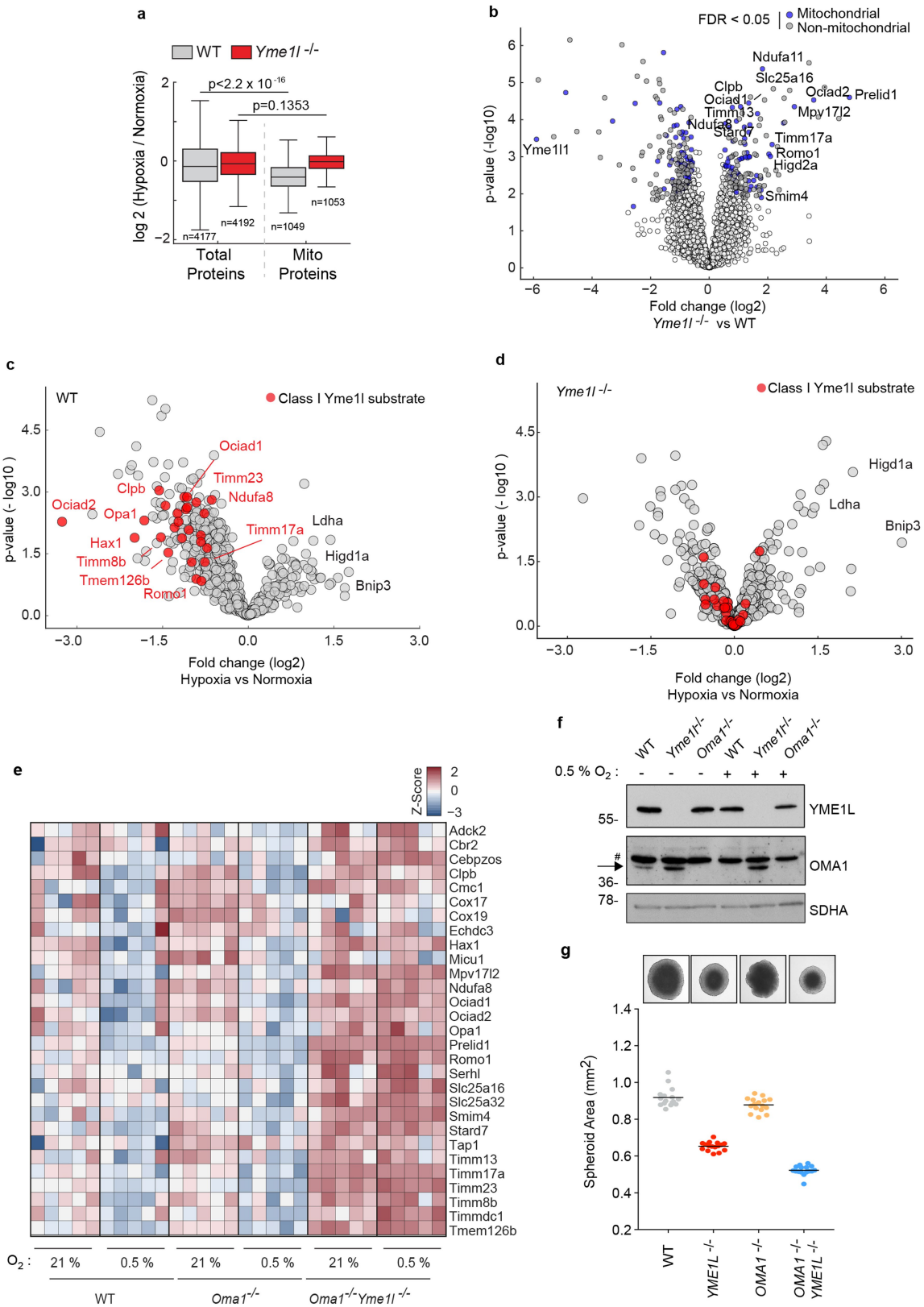
Extended Data Fig. 1 | Characterization of YME1L-dependent spheroid growth. **a, b**, Spheroid surface area (**a**) and ATP levels (**b**) of HEK293 cell lines after 7 days of culture (**a**, $n=5$ independent experiments; **b**, $n=3$ independent experiments; # is number of spheroids per condition). **c, d**, Spheroid surface area (**c**) and ATP content (**d**) of WT and $YME1L^{-/-}$ HeLa cells after 7 days ($n=3$ independent experiments; # is number of spheroids per condition). **e**, Quantification of the NAD/NADH ratio in WT and $YME1L^{-/-}$ HEK293 cells cultured in normoxia (21% O_2) or hypoxia (0.5% O_2) for 24 h ($n=3$ independent experiments). **f**, Spheroid surface area of WT and $YME1L^{-/-}$ HEK293 cells and of $YME1L^{-/-}$ HEK293 cells expressing Lb-NOX (NADH oxidase from *Lactobacillus brevis*)⁴⁷ after 7 days ($n=1$ experiment; # is number of spheroids per condition).

The expression of Lb-NOX was determined by SDS-PAGE and immunoblotting of control and Lb-NOX-expressing WT and $YME1L^{-/-}$ HEK293 cells in normoxia (21% O_2) or hypoxia (0.5% O_2) for 24 h. **g**, The dependency of WT and $YME1L^{-/-}$ HEK293 cells on glucose oxidation (left) and fatty acid oxidation (right) was monitored using the XF Fuel Flex Assay. Dependencies are calculated as a percentage of combined glucose, fatty acid and glutamine oxidation ($n=4$ independent experiments). **h–j**, Quantification of cellular metabolites from HEK293 cells (**h, i**) and MEFs (**j**). Metabolite abundance was normalized to those of WT cells ($n=5$ independent experiments). Mean \pm s.e.m.; one-way ANOVA with Dunnett's multiple comparisons test (**a, b**); two tailed *t*-test (**c, d, g**); two-way ANOVA with Sidak's multiple comparisons test (**e**).



Extended Data Fig. 2 | HIF1α drives YME1L-dependent proteolysis and occurs independently of mitophagy. **a**, SDS-PAGE and immunoblot analysis of WT and *YME1L*^{-/-} HEK293 cells expressing YME1L or YME1L(E543Q) cultured for 7 days as monolayers (M) or spheroids (S) ($n=1$ experiment). **b**, Representative immunoblot of WT and *YME1L*^{-/-} HEK293 cells and *YME1L*^{-/-} HEK293 cells expressing YME1L or YME1L(E543Q) cultured in normoxia (21% O₂) or hypoxia (0.5% O₂) for 16 h ($n=4$ independent experiments). **c**, SDS-PAGE and immunoblot analysis of the indicated cell lines treated with control (Scr) or *Yme1* siRNA and incubated in normoxia (21% O₂) or hypoxia (0.5% O₂) for 16 h ($n=1$ experiment). **d**, SDS-PAGE and immunoblot analysis of WT and *YME1L*^{-/-} cells treated with Co(II)Cl₂ (200 μ M) for 24 h or DFP (1 mM) for 24 h. Quantification of PRELID1 and TIMM23 protein levels is shown ($n=3$ independent experiments; fc, fold change). **e**, Quantified PRELID1 and TIMM17A protein levels in HeLa cells transfected with *Gfp* or *Hif1α* esiRNA cultured in normoxia or hypoxia for 24 h (example blot shown in Fig. 1f; $n=3$ independent experiments; fc, fold change). **f**, SDS-PAGE and immunoblot analysis of WT and *Atg5*^{-/-} MEFs cultured in hypoxia (0.5% O₂) for the indicated time. Quantification of PRELID1 and TIMM23 protein levels is shown ($n=3$ independent experiments; fc, fold change). Mean \pm s.e.m.; two-way ANOVA with Sidak's multiple comparisons test (e).

HEK293 cells treated with Co(II)Cl₂ (200 μ M) for 24 h or DFP (1 mM) for 24 h. Quantification of PRELID1 and TIMM23 protein levels is shown ($n=3$ independent experiments; fc, fold change). **e**, Quantified PRELID1 and TIMM17A protein levels in HeLa cells transfected with *Gfp* or *Hif1α* esiRNA cultured in normoxia or hypoxia for 24 h (example blot shown in Fig. 1f; $n=3$ independent experiments; fc, fold change). **f**, SDS-PAGE and immunoblot analysis of WT and *Atg5*^{-/-} MEFs cultured in hypoxia (0.5% O₂) for the indicated time. Quantification of PRELID1 and TIMM23 protein levels is shown ($n=3$ independent experiments; fc, fold change). Mean \pm s.e.m.; two-way ANOVA with Sidak's multiple comparisons test (e).



Extended Data Fig. 3 | See next page for caption.

Article

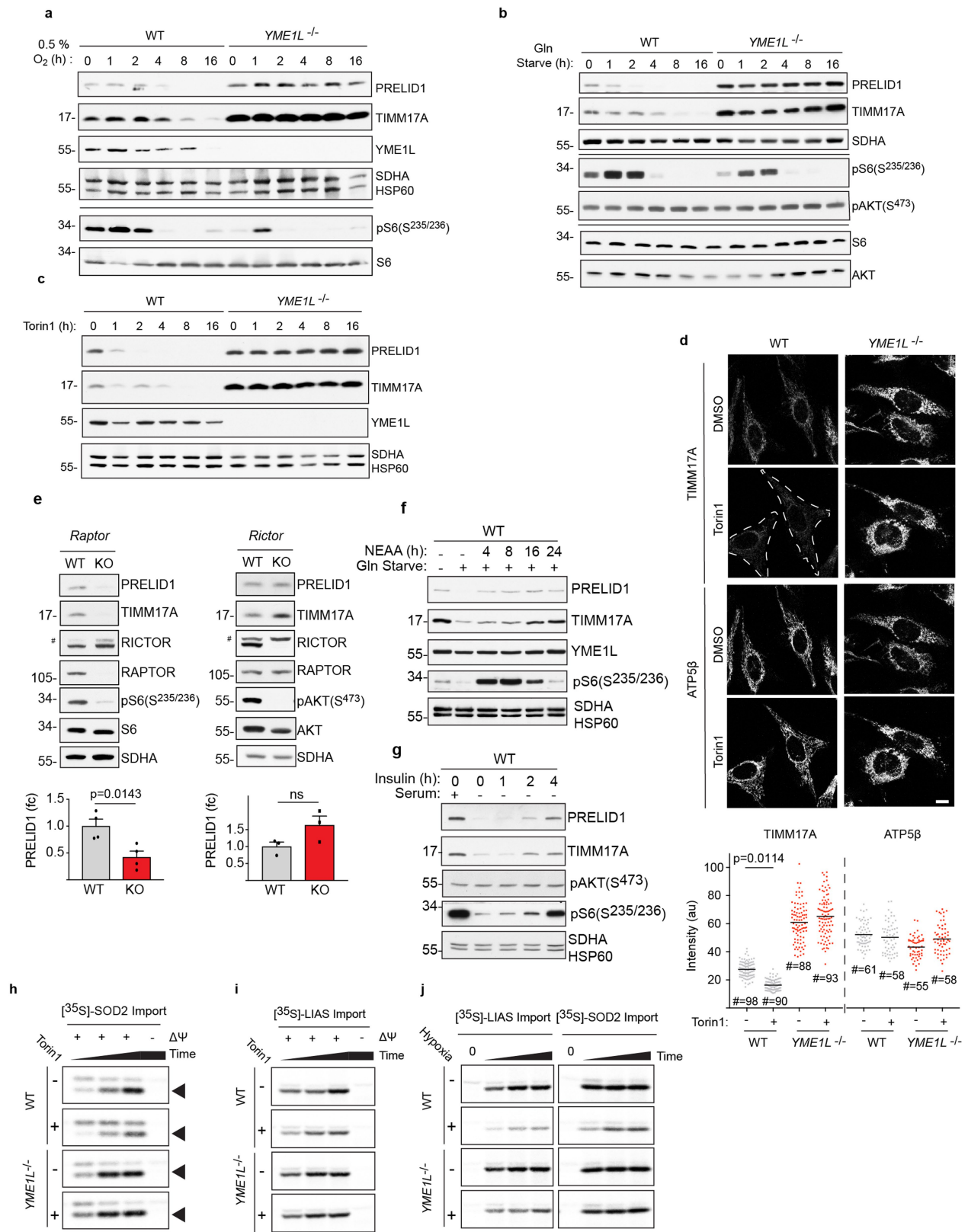
Extended Data Fig. 3 | YME1L reshapes the mitochondrial proteome

independently of OMA1. **a**, Box plot analysis of the \log_2 ratio distribution comparing hypoxia and normoxia in WT and *Yme1l*^{-/-} MEFs of total proteins and mitochondrial proteins. *P* values calculated by Wilcoxon sum-rank test. Centre lines denote medians, box limits denote 25th and 75th percentiles; whiskers denote maxima and minima (1.5 times the interquartile range). Data located outside the maxima or minima were denoted as outliers and removed.

b, Volcano plot representation of proteins determined by quantitative mass spectrometry after isolation of mitochondria from WT and *Yme1l*^{-/-} MEFs cultivated under normoxic conditions (dataset as in Fig. 1g, $n=5$ independent experiments, two-tailed *t*-test). Filled plots indicate proteins that differ significantly between *Yme1l*^{-/-} and WT MEFs at a permutation-based estimated FDR < 0.05. Among these, mitochondrial proteins (according to Gene Ontology

Cellular Component) are highlighted in blue. Mitochondrial proteins enriched in *Yme1l*^{-/-} compared to WT are putative YME1L substrates (class I or II).

c, d, Volcano plots of mitochondrial protein changes in hypoxia versus normoxia from WT (c) or *Yme1l*^{-/-} (d) MEFs (dataset as in Fig. 1g, $n=5$ independent experiments, two-tailed *t*-test). Class I YME1L substrates are highlighted in red. **e**, Z-score of \log_2 -transformed LFQ intensities of class I YME1L substrates in WT, *Oma1*^{-/-} and *Oma1*^{-/-} *Yme1l*^{-/-} MEFs treated as in Fig. 1g ($n=5$ independent experiments). **f**, SDS-PAGE and immunoblot analysis of WT, *Yme1l*^{-/-} and *Oma1*^{-/-} MEFs cultured in normoxia (21% O₂) or hypoxia (0.5% O₂) for 24 h. # denotes nonspecific cross-reaction ($n=1$ experiment). **g**, Spheroid surface area of the indicated HEK293 cell lines after 7 days (means from 16 spheroids shown, $n=1$ experiment).

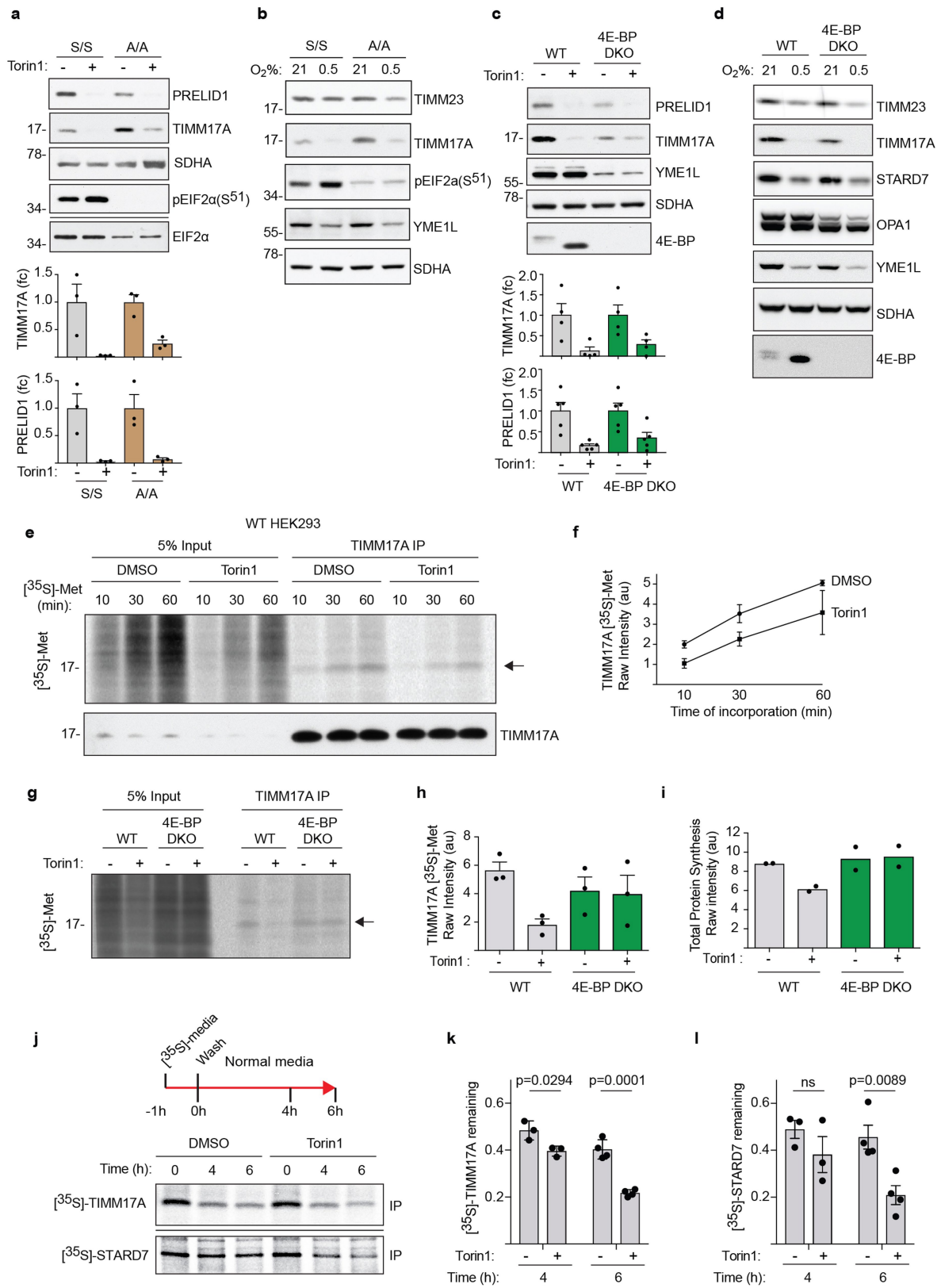


Extended Data Fig. 4 | See next page for caption.

Article

Extended Data Fig. 4 | mTORC1 acutely regulates YME1L-dependent proteolysis and mitochondrial import. **a–c**, SDS–PAGE and immunoblot analysis of WT and *YME1L*^{−/−} HEK293 cells cultured in hypoxia (0.5% O₂) (**a**), glutamine-depleted medium (**b**) or in the presence of 400 nM Torin1 (**c**) for the indicated times (representative immunoblots from *n* = 3 independent experiments, quantification shown in Fig. 2b). **d**, Immunofluorescence of WT and *YME1L*^{−/−} HeLa cells treated with Torin1 (400 nM) for 4 h. Cells were immunostained with TIMM17A- and ATP5 β -specific antibodies. Quantification of mean fluorescence intensity per cell is shown (TIMM17A mean from three independent experiments, two-way ANOVA with Sidak multiple comparisons test; ATP5 β mean from two independent experiments). # is number of cells per condition; au, arbitrary unit; scale bar, 10 μ m. **e**, Immunoblot of WT, *Raptor* and *Rictor* knockout (KO) MEFs. Quantified PRELID1 protein levels are shown (*Raptor*, *n* = 4 independent experiments; *Rictor*, *n* = 3 independent experiments; mean \pm s.e.m.; two-tailed *t*-test). fc, fold change. # denotes nonspecific cross-reaction. **f**, HEK293 cells were cultured in glutamine-depleted medium (Starve)

for 16 h and then cultured in non-essential amino acid (NEAA)-containing medium for the indicated time. Cell lysates were analysed by SDS–PAGE and immunoblotting (*n* = 1 experiment). **g**, HEK293 cells were cultured in serum-depleted medium for 16 h and treated with insulin (100 nM) for the indicated time. Cell lysates were analysed by SDS–PAGE and immunoblotting (*n* = 1 experiment). **h, i**, [³⁵S]-SOD2 (**h**) and [³⁵S]-LIAS (**i**) were imported into mitochondria isolated from WT and *YME1L*^{−/−} HEK293 cells treated with or without 400 nM Torin1 for 18 h. Import was stopped after 1.5, 3 and 4.5 min in the presence or absence of membrane potential ($\Delta\psi$). Mitochondria were analysed by SDS–PAGE and autoradiography (representative blots from *n* = 2 (**h**) and *n* = 3 (**i**) independent experiments). Arrows indicate the mature form of SOD2. **j**, [³⁵S]-LIAS and [³⁵S]-SOD2 were imported into mitochondria isolated from WT and *YME1L*^{−/−} HEK293 cells incubated in normoxia (21% O₂) or hypoxia (0.5% O₂) for 18 h. Import was stopped after 5, 10 and 15 min. Mitochondria were analysed by SDS–PAGE and levels of imported [³⁵S]-LIAS and [³⁵S]-SOD2 were observed by autoradiography (*n* = 1 experiment).

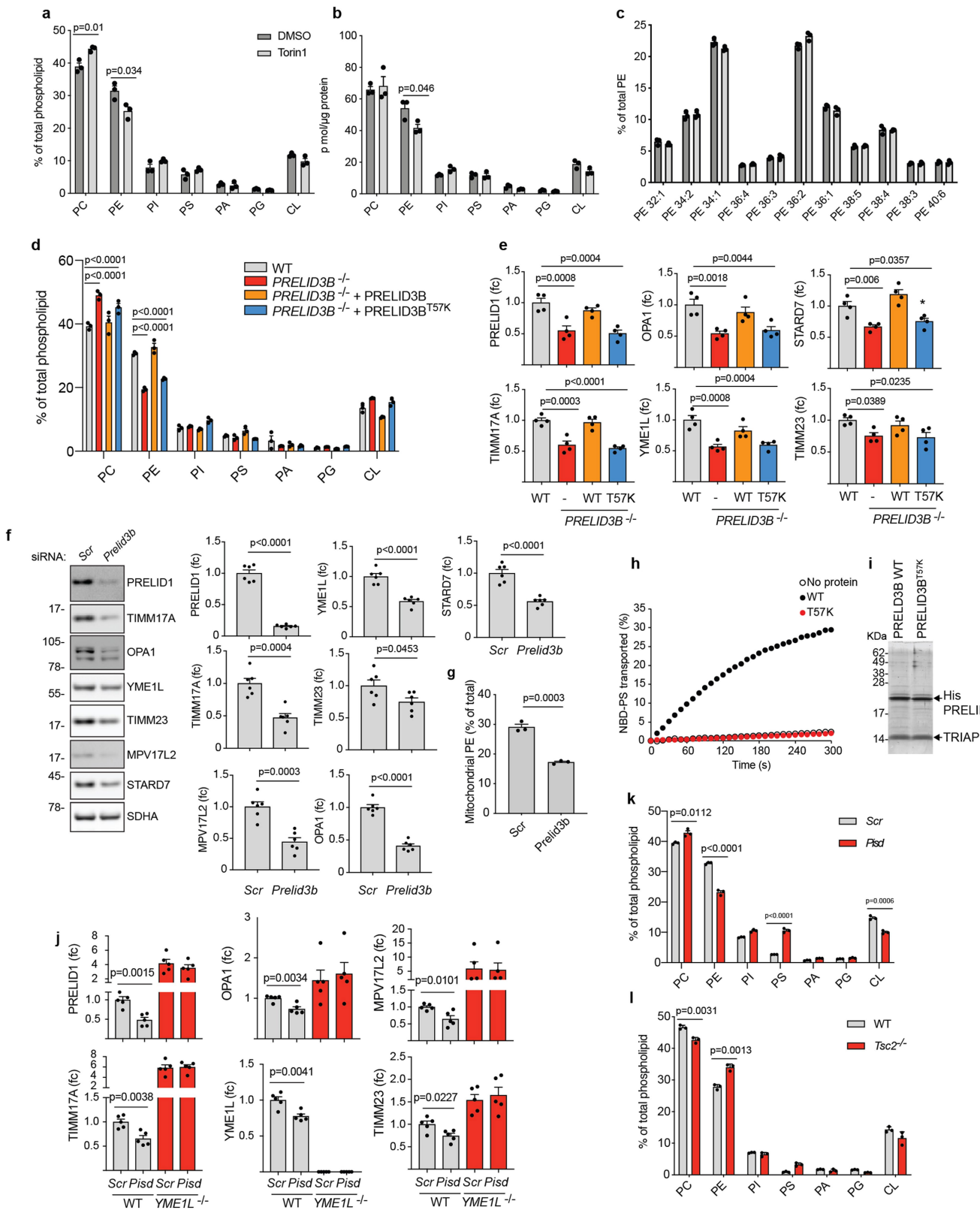


Extended Data Fig. 5 | See next page for caption.

Article

Extended Data Fig. 5 | mTORC1 regulates YME1L-mediated proteolysis in a post-translational manner. **a, b**, YME1L degradation of substrates does not depend on EIF2 α phosphorylation and integrated stress response (ISR) activation. SDS-PAGE and immunoblot analysis of WT (S/S) and EIF2 α^{SS1A} knock-in (A/A) MEFs, which cannot activate the ISR⁴⁸, treated with Torin1 for 4 h (**a**; $n = 3$ independent experiments, mean \pm s.e.m.) or cultured in normoxia (21% O₂) or hypoxia (0.5% O₂) for 24 h (**b**; $n = 3$ independent experiments). **c, d**, YME1L degradation of substrates does not depend on mTORC1 regulation of translation initiator factor 4 binding proteins (4E-BPs). SDS-PAGE and immunoblot analysis of WT and *Eif4ebp1^{-/-}Eif4ebp2^{-/-}* (4E-BP DKO) MEFs treated with Torin1 for 4 h (**c**; $n = 4$ independent experiments, mean \pm s.e.m.) or cultured in normoxia (21% O₂) or hypoxia (0.5% O₂) for 16 h (**d**; $n = 3$ independent experiments). **e, f**, We observed a slight reduction in newly synthesized TIMM17A in Torin1-treated WT HEK293 cells, consistent with previous reports⁴⁹. After treatment with DMSO or Torin1 for 2 h, cells were incubated in labelling medium containing [³⁵S]-methionine for the indicated time before lysis and immunoprecipitation with an antibody targeting TIMM17A. Input (5% of total) and immunoprecipitates (IP) were analysed by SDS-PAGE and autoradiography. [³⁵S]-TIMM17A (indicated by an arrow) was quantified (**f**). Total TIMM17A protein level was determined by immunoblotting ($n = 3$ independent experiments, mean \pm s.e.m.). au, arbitrary unit. **g–i**, TIMM17A

synthesis and the majority of global translation was restored in Torin1-treated MEFs that lack 4E-BP proteins. This confirms that the reduced synthesis of TIMM17A upon mTORC1 inhibition reflects 4E-BP-dependent attenuation of translation⁴⁹. After treatment with DMSO or Torin1 for 2 h, cells were incubated in labelling medium containing [³⁵S]-methionine for 60 min before lysis and immunoprecipitation with an antibody targeting TIMM17A. TIMM17A levels (**h**) were analysed and quantified as in **f** ($n = 3$ independent experiments, mean \pm s.e.m.). Total protein synthesis was determined by the intensity of all bands in input lanes (**i**) ($n = 2$ independent experiments). The synthesis rate of TIMM17A was quantified in WT and *Eif4ebp1^{-/-}Eif4ebp2^{-/-}* (4E-BP DKO) MEFs. au, arbitrary unit. **j–l**, Post-translational degradation of YME1L substrates monitored by [³⁵S]-methionine pulse-chase experiment in HEK293 cells. After labelling for 1 h in [³⁵S]-methionine containing medium, cells were incubated for 4 h and 6 h in radioactive-free medium in the presence and absence of Torin1. [³⁵S]-labelled TIMM17A and STARD7 were immunoprecipitated and their levels determined by SDS-PAGE and autoradiography. Quantification of the fraction of [³⁵S]-TIMM17A (**k**) and [³⁵S]-STARD7 (**l**) remaining after 4 and 6 h chase is shown. Torin1 treatment accelerated TIMM17A and STARD7 degradation ($n = 3$ independent experiments for 4 h, $n = 4$ independent experiments for 6 h; mean \pm s.e.m.; two tailed *t*-test).



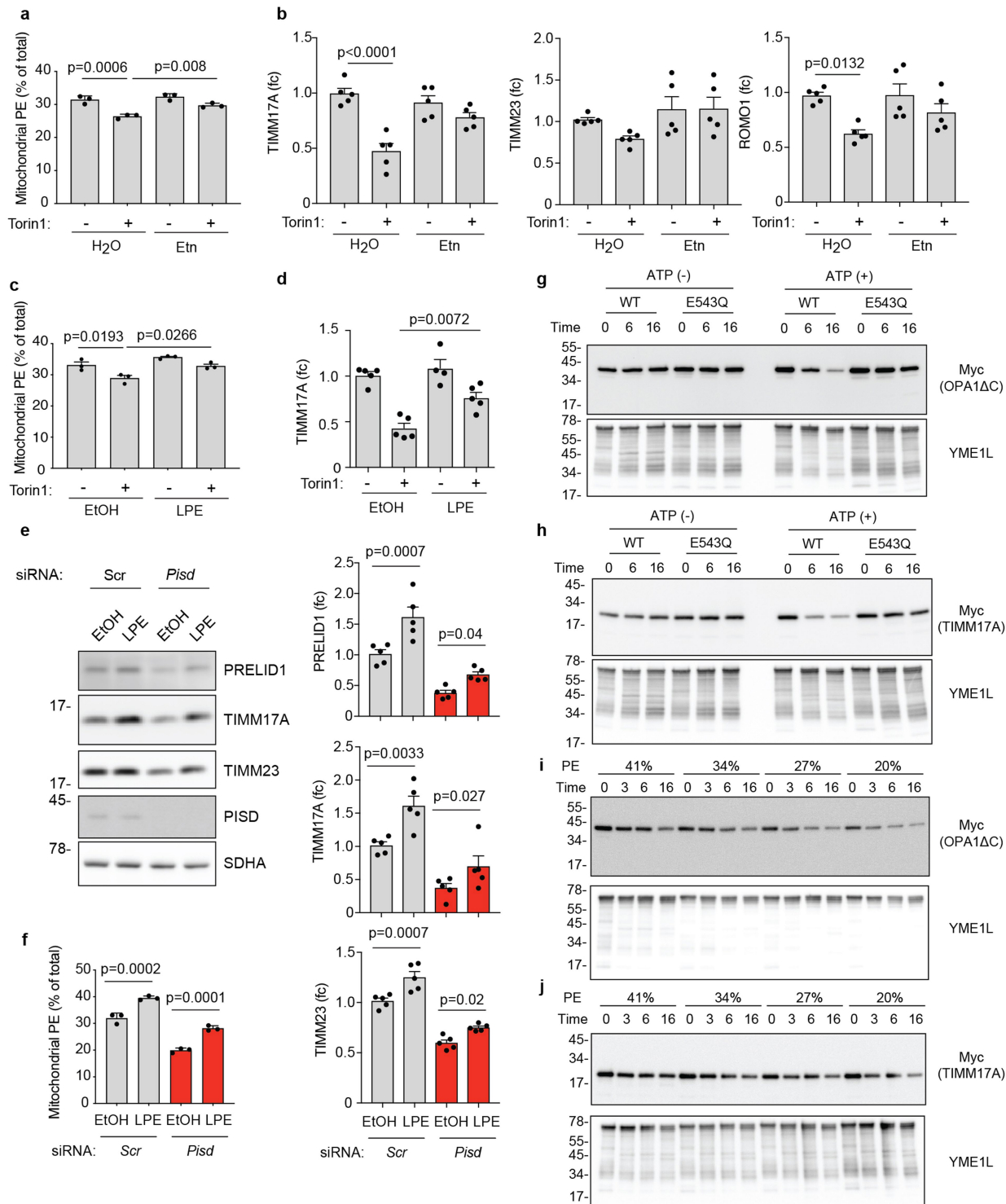
Extended Data Fig. 6 | See next page for caption.

Article

Extended Data Fig. 6 | Decreased mitochondrial PE promotes YME1L-mediated proteolysis. **a, b**, Phospholipid analysis of mitochondrial fractions from HeLa cells treated with Torin1 for 4 h ($n=3$ independent experiments); **a**, relative distribution; **b**, absolute abundance. **c**, Acyl chain composition of mitochondrial PE from HeLa cells treated with Torin1 for 4 h ($n=3$ independent experiments). **d**, Phospholipid analysis of mitochondrial fractions from WT, *PRELID3B*^{-/-} and *PRELID3B*^{+/+} HeLa cells expressing PRELID3B-Flag or PRELID3B(T57K)-Flag ($n=3$ independent experiments). **e**, Quantification of protein levels from Fig. 2h ($n=4$ independent experiments). **f, g**, Immunoblot and mitochondrial phospholipid analysis of scrambled control (*Scr*) or *Prelid3b* siRNA-transfected HeLa cells. Quantification of indicated protein levels is shown (immunoblot, $n=6$ independent experiments; phospholipid analysis, $n=3$ independent experiments). **h**, NBD-PS transfer by PRELID3B (black

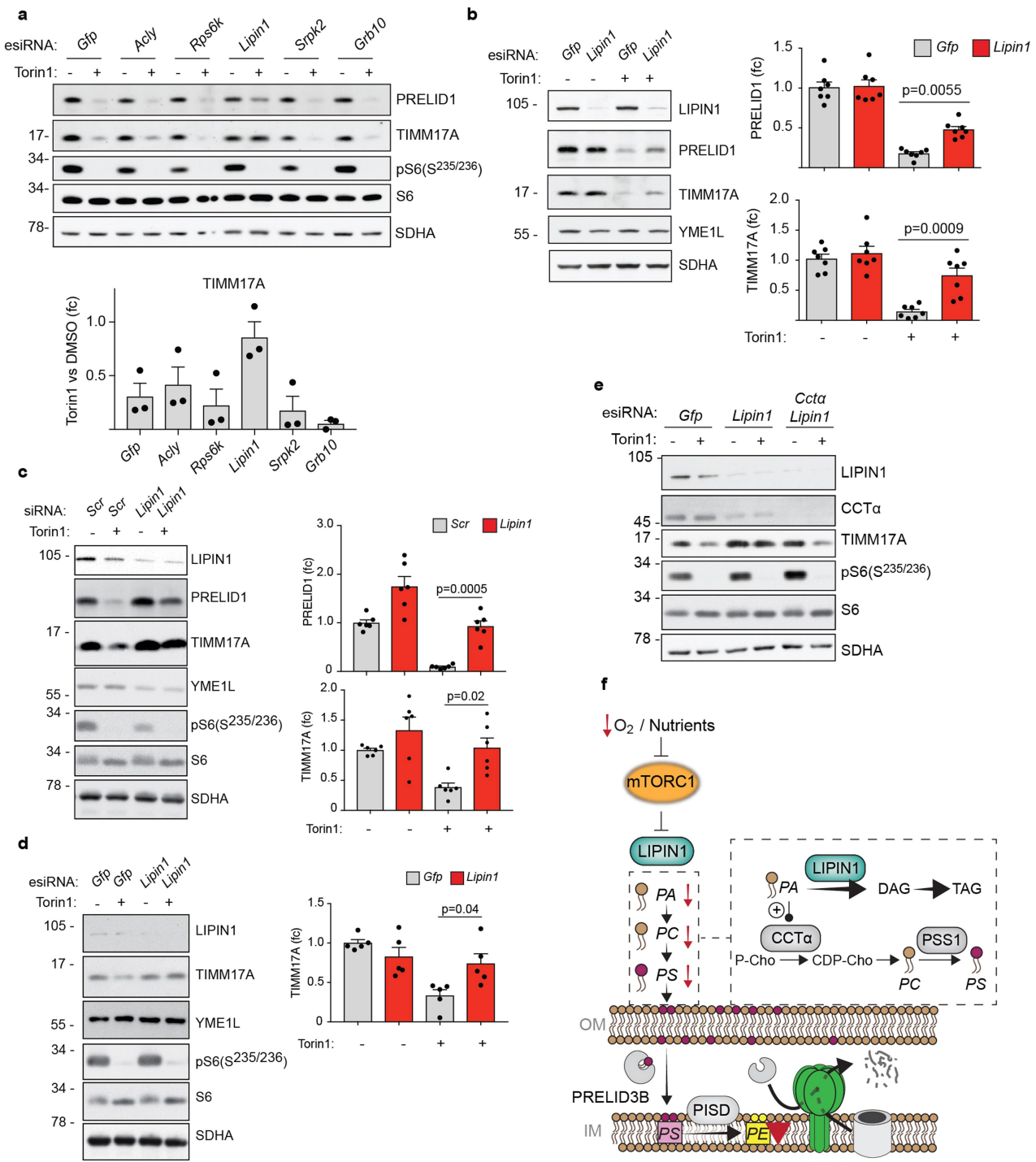
circles), PRELID3B(T57K) (red circles) or without addition of protein (white circles). PRELID3B(T57K) contains a mutation in the PS-binding site, which abolishes PS transfer but does not interfere with the assembly of PRELID3B into lipid transfer complexes. Average of $n=3$ independent experiments.

i, SDS-PAGE analysis of recombinant PRELID3B-TRIAP1 complexes and the T57K variant (40 pmol) by CBB staining ($n=1$ experiment). **j**, Quantification of protein levels from Fig. 2i ($n=5$ independent experiments). **k, l**, Phospholipid analysis of the mitochondrial fraction from HeLa cells treated with scrambled control (*Scr*) or *Pisd* siRNA ($n=3$ independent experiments) (**k**), WT and *Tsc2*^{-/-} MEFs ($n=3$ independent experiments) (**l**). Mean \pm s.e.m.; two tailed *t*-test (**a, b, f, g, j–l**), one-way ANOVA with Dunnett's multiple comparisons test (**d, e**). fc, fold change.



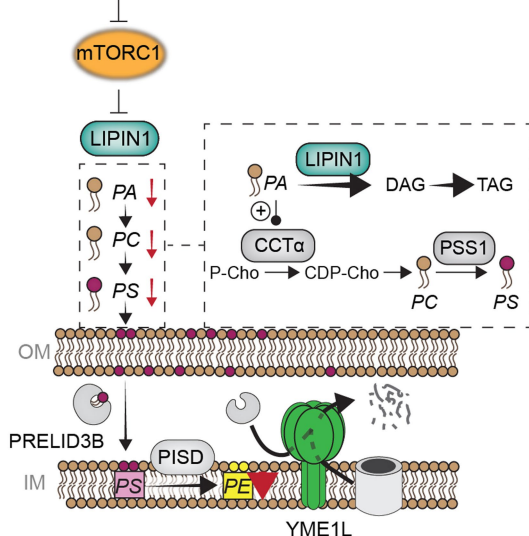
Extended Data Fig. 7 | PE regulates YME1L-mediated proteolysis. **a, b**, HeLa cells pretreated with ethanolamine (Etn, 200 μ M) for 24 h were treated with Torin1 for 4 h. Phospholipids in mitochondrial fractions were analysed by mass spectrometry (a) ($n=3$ independent experiments). Cell lysates were analysed by immunoblotting and indicated protein levels were quantified ($n=5$ independent experiments) (b). **c, d**, HEK293 cells were treated with Torin1 and/or 100 μ M LPE for 4 h. Phospholipids in mitochondrial fractions were analysed by mass spectrometry (c) ($n=3$ independent experiments). Cell lysates were analysed by immunoblotting and indicated protein levels were quantified ($n=4-5$ independent experiments) (d). **e, f**, HeLa cells transfected with scrambled control (Scr) or Pisd siRNA were treated with 100 μ M LPE for 24 h. Cell lysates were analysed by immunoblotting and indicated protein levels

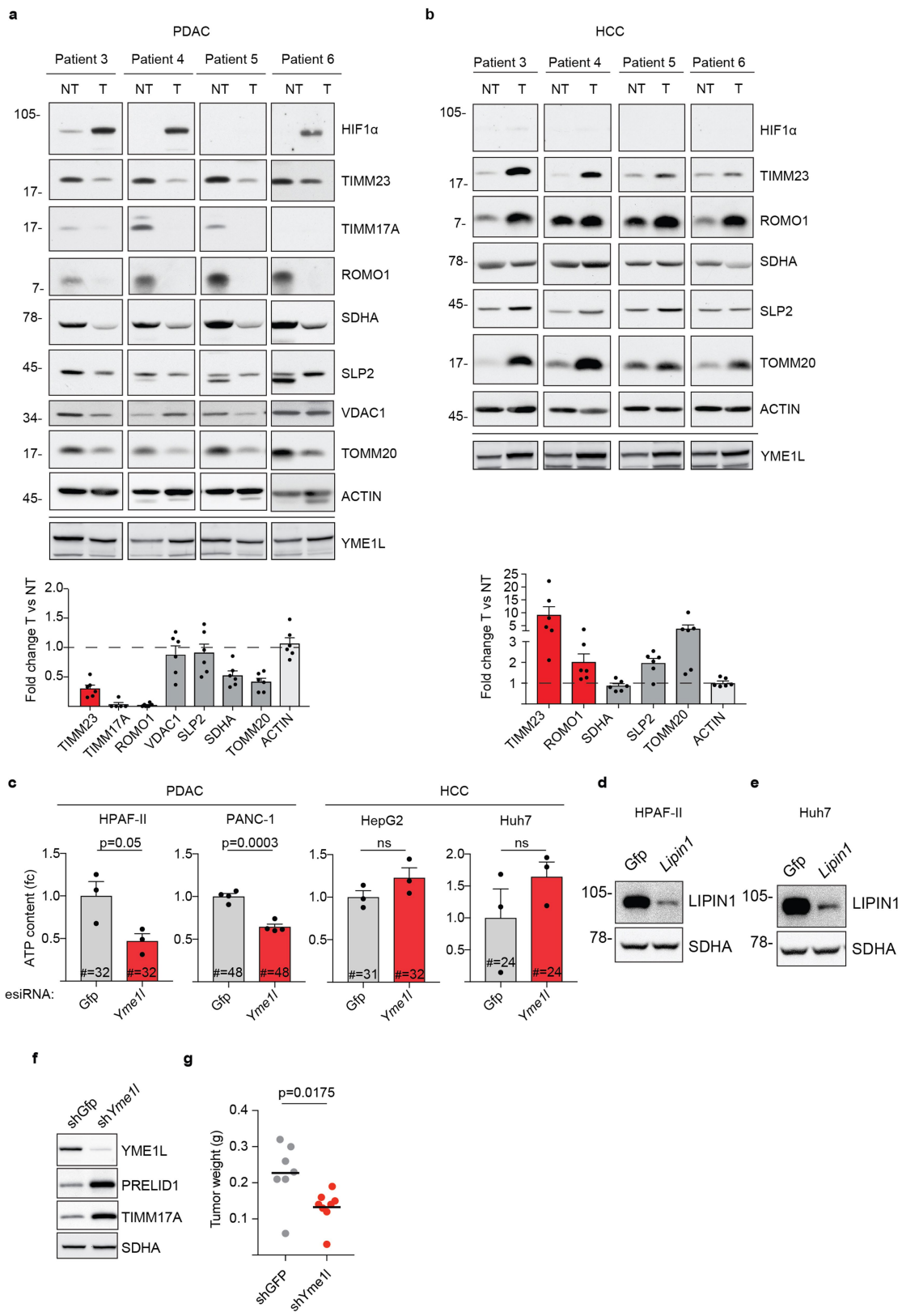
were quantified ($n=5$ independent experiments) (e). PE levels in mitochondrial fractions were determined by mass spectrometry ($n=3$ independent experiments) (f). **g, h**, YME1L (WT or E543Q) and OPA1ΔC (g) or TIMM17A (h) reconstituted in liposomes was incubated in the presence or absence of ATP at 37 °C for the indicated times. Samples were analysed by immunoblotting (representative data from $n=3$ independent experiments). **i, j**, YME1L (WT or E543Q) and OPA1ΔC (i) or TIMM17A (j) reconstituted in liposomes containing different amounts of PE were incubated in the presence of ATP at 37 °C for the indicated times. Samples were analysed by immunoblotting (representative data from $n=4$ independent experiments). Mean \pm s.e.m.; two-way ANOVA with Tukey's multiple comparisons test (a-d), with Holm-Sidak's multiple comparisons test (e, f). fc, fold change.



Extended Data Fig. 8 | Depletion of LIPIN1 preserves YME1L-mediated proteolysis after inhibition of mTORC1. **a**, HeLa cells transfected with the indicated esiRNAs were treated with Torin1 for 4 h before immunoblotting. Representative immunoblot and quantification of TIMM17A protein levels are shown ($n=3$ independent experiments; fold change (fc) from DMSO control). **b, c**, Immunoblot analysis of HeLa cells transfected with *Gfp* or *Lipin1* esiRNA (**b**) or scrambled control (*Scr*) or *Lipin1* siRNA (**c**) treated with Torin1 for 4 h. Quantification of PRELID1 and TIMM17A protein levels is shown ($n=6$ independent experiments (**b**), $n=7$ independent experiments (**c**)). **d**, Immunoblot analysis of MEFs transfected with *Gfp* or *Lipin1* esiRNA and

treated with Torin1 for 4 h. Quantification of TIMM17A protein levels is shown ($n=5$ independent experiments). **e**, Immunoblot analysis of HeLa cells transfected with the indicated esiRNAs and treated with Torin1 for 4 h (representative data from six independent experiments). **f**, The mTORC1-LIPIN1-YME1L regulatory axis. Upon inhibition of mTORC1, dephosphorylation of LIPIN1 stimulates its PA-phosphatase activity and leads to a decrease in PA. The depletion of PA inhibits CCT α and therefore limits the supply of PS to mitochondria. Reduced PS transfer to the inner membrane limits accumulation of PE, stimulating YME1L-mediated proteolysis. Mean \pm s.e.m.; two-way ANOVA with Tukey's multiple comparisons test (**b-d**).





Extended Data Fig. 9 | See next page for caption.

Article

Extended Data Fig. 9 | YME1L-mediated proteolysis is enhanced in PDAC and supports the growth of PDAC cells. **a, b**, SDS-PAGE and immunoblot analysis of pancreatic tissue from patients with PDAC (**a**) and liver tissue from patients with HCC (**b**). T, tumour tissue; NT, corresponding adjacent non-tumour tissue. Quantification of indicated protein levels is shown below ($n = 6$ independent patient samples). YME1L substrate proteins are highlighted in red, other mitochondrial proteins shown in dark grey. The immunoblots from two other patients are shown in Fig. 4a, b, c. **c**, Cellular ATP levels in spheroids of the indicated cell lines cultured for 6 days ($n = 3$ independent experiments for

HPAF-II, HepG2 and Huh7, $n = 4$ independent experiments for PANC1; # is number of spheroids; fc, fold change). **d, e**, Immunoblot analysis of spheroids from HPAF-II (**d**) and Huh7 (**e**) cells treated with *Gfp* or *Lipin1* esiRNA, quantified in Fig. 4e, f, $n = 1$ immunoblot. **f**, Representative immunoblot of HPAF-II cells expressing sh*Gfp* and sh*Yme1l* ($n = 3$ independent samples). **g**, Weights of xenograft tumours derived from HPAF-II cells treated with *Gfp* or *Yme1l* shRNA 28 days after injection (*Gfp* $n = 7$ mice; *Yme1l* $n = 8$ mice). Mean \pm s.e.m.; two tailed unpaired *t*-test (**a–c, g**).

Extended Data Table 1 | Class I and class II YME1L substrates

Mitochondrial Function	Protein	Fold change (log2)	p-value (-log10)	Compartment	Class
Import	Timm17a	2.15	3.33	IM	I
	Romo1	2.04	3.07	IM	I
	Timm22	1.43	2.2	IM	II
	Timm13	0.93	3.96	IMS	I
	Timm8b	0.75	2.62	IMS	I
	Timm23	0.67	2.96	IM	I
Lipid Transport	Prelid1	4.79	4.6	IMS	I
	Triap1	1.65	4.16	IMS	II
	Nme4	1.22	3.34	IMS	II
	Stard7	1.2	3.8	IMS	I
Dynamics	Opa1	1.76	2.42	IM + IMS	I
	Mtrf2	0.96	2.55	?	II
	Mief1	NaN	NaN	OM	II
Respiration	Tmem126b	2.54	3.91	IM	I
	Higd2a	2.09	3.01	IM	II
	Ndufa11	1.82	5.37	IM	II
	Smim4	1.78	1.9	IM	I
	Pet117	1.37	2.1	IM	II
	Timmdc1	1	2.54	IM	I
	Cox19	0.81	2.4	IM	I
	Cox17	0.79	2.71	IMS	I
	Ociad1	0.79	4.33	IM	I
	Ndufa8	0.68	3.79	IMS	I
	Surf1	0.6	2.74	IM	II
	Cmc1	0.56	2.77	IMS	I
Solute carriers and ABC transporters	Slc25a33	1.63	2.18	IM	II
	Slc25a16	1.35	4.45	IM	I
	Abcb6	1.31	2.97	IM + OM	II
	Abcb1b	1.29	3.11		II
	Slc25a25	1.21	3.49	IM	II
	Slc25a32	1.1	2.95	IM	I
	Abcq2	0.91	3.07	IM	II
	Slc25a28	NaN	NaN	IM	II
	Slc25a38	NaN	NaN	IM	II
	Ass1	1.77	2.1	?	II
Metabolism	Cbr2	1.39	3.86	Matrix	I
	Echdc3	1.35	3.66	?	I
	Akr1b10	1.24	2.99	?	II
	Gpam	1.1	2.14	OM	II
	Dglicy	0.93	2.16	Matrix	II
	Serhl	0.88	2.37	?	I
	Sqrdl	0.72	2.5	IM	II
	Nudt19	0.68	2.74	?	II
	Nnt	0.63	2.86	IM	II
	Oxct1	0.56	3.9	Matrix	II
	Cmpk2	NaN	NaN	Matrix	II
	Ldhb	NaN	NaN	?	II
	Pnpla7	NaN	NaN	?	II
	Sfxn4	NaN	NaN	IM	II
Other and Unknown	Ociad2	3.57	4.53	?	I
	Mpv17l2	2.91	4.35	IM	I
	Hrsp12	1.62	2.49	Matrix	II
	Tmem173	1.52	2.36		II
	Hax1	1.38	3	IM	I
	Adck2	1.37	3	?	I
	Tap1	1.35	2.35	?	I
	Cebpzos	1.19	3.39	IMS	I
	Clpb	1.07	4.35	IMS	I
	Fundc2	1.02	2.92	OM	II
	Araf	0.93	2.04	?	II
	Micu1	0.56	2.74	IMS	I
	Fam136a	0.54	3.18	?	II
	Fundc1	NaN	NaN	OM	II
	Wasf1	NaN	NaN	?	II

Class I and II YME1L substrate proteins grouped according to function. Protein level fold changes (\log_2) in *Yme1l^{-/-}* compared to WT MEFs in normoxia are shown. NaN indicates that the protein was exclusively quantified in *Yme1l^{-/-}* cells and a fold change could therefore not be determined.

Reporting Summary

Nature Research wishes to improve the reproducibility of the work that we publish. This form provides structure for consistency and transparency in reporting. For further information on Nature Research policies, see [Authors & Referees](#) and the [Editorial Policy Checklist](#).

Statistical parameters

When statistical analyses are reported, confirm that the following items are present in the relevant location (e.g. figure legend, table legend, main text, or Methods section).

n/a Confirmed

- The exact sample size (n) for each experimental group/condition, given as a discrete number and unit of measurement
- An indication of whether measurements were taken from distinct samples or whether the same sample was measured repeatedly
- The statistical test(s) used AND whether they are one- or two-sided
Only common tests should be described solely by name; describe more complex techniques in the Methods section.
- A description of all covariates tested
- A description of any assumptions or corrections, such as tests of normality and adjustment for multiple comparisons
- A full description of the statistics including central tendency (e.g. means) or other basic estimates (e.g. regression coefficient) AND variation (e.g. standard deviation) or associated estimates of uncertainty (e.g. confidence intervals)
- For null hypothesis testing, the test statistic (e.g. F , t , r) with confidence intervals, effect sizes, degrees of freedom and P value noted
Give P values as exact values whenever suitable.
- For Bayesian analysis, information on the choice of priors and Markov chain Monte Carlo settings
- For hierarchical and complex designs, identification of the appropriate level for tests and full reporting of outcomes
- Estimates of effect sizes (e.g. Cohen's d , Pearson's r), indicating how they were calculated
- Clearly defined error bars
State explicitly what error bars represent (e.g. SD, SE, CI)

Our web collection on [statistics for biologists](#) may be useful.

Software and code

Policy information about [availability of computer code](#)

Data collection

No software was used.

Data analysis

LipidView Software Version 1.2
Prism GraphPad 8 Software RRID:SCR_002798 Version 8.20
ImageJ National Institutes of Health 1.48u; RRID:SCR_003070
InstantClue Nolte et al., 2018 <http://www.instantclue.uni-koeln.de/> Version 0.5.3
Wave controller Version 2.2.0 Agilent Technologies

For manuscripts utilizing custom algorithms or software that are central to the research but not yet described in published literature, software must be made available to editors/reviewers upon request. We strongly encourage code deposition in a community repository (e.g. GitHub). See the Nature Research [guidelines for submitting code & software](#) for further information.

Data

Policy information about [availability of data](#)

All manuscripts must include a [data availability statement](#). This statement should provide the following information, where applicable:

- Accession codes, unique identifiers, or web links for publicly available datasets
- A list of figures that have associated raw data
- A description of any restrictions on data availability

The accession number for the proteomics data reported in this paper in Fig. 1 and Extended Data Fig. 3 is PRoteomics IDEntifications (PRIDE): PXD011750.

The accession number for the proteomics data reported in this paper in Fig. 2 is PRoteomics IDEntifications (PRIDE): PXD014405.

The GEO omnibus accession number for the RNA sequence data reported in this paper in Fig. 1k is GSE133753

Field-specific reporting

Please select the best fit for your research. If you are not sure, read the appropriate sections before making your selection.

Life sciences Behavioural & social sciences Ecological, evolutionary & environmental sciences

For a reference copy of the document with all sections, see nature.com/authors/policies/ReportingSummary-flat.pdf

Life sciences study design

All studies must disclose on these points even when the disclosure is negative.

Sample size	Sample size was chosen according to our previous experience. No statistical method was used to predetermine sample size. The sample size included at least 3 biological replicates where statistical evaluation was performed.
Data exclusions	We have not excluded any samples from our studies.
Replication	Experiments were repeated as detailed in the figure legends. All attempts at replication were successful. In some cases, multiple cell lines were used to verify the reproducibility of the findings.
Randomization	Mice were randomly assigned to experimental groups after purchase.
Blinding	Analyses were not blinded because experiments were performed and analyzed by the same researchers.

Reporting for specific materials, systems and methods

Materials & experimental systems

n/a	Involved in the study
<input type="checkbox"/>	<input checked="" type="checkbox"/> Unique biological materials
<input type="checkbox"/>	<input checked="" type="checkbox"/> Antibodies
<input type="checkbox"/>	<input checked="" type="checkbox"/> Eukaryotic cell lines
<input checked="" type="checkbox"/>	<input type="checkbox"/> Palaeontology
<input type="checkbox"/>	<input checked="" type="checkbox"/> Animals and other organisms
<input checked="" type="checkbox"/>	<input type="checkbox"/> Human research participants

Methods

n/a	Involved in the study
<input checked="" type="checkbox"/>	<input type="checkbox"/> ChIP-seq
<input checked="" type="checkbox"/>	<input type="checkbox"/> Flow cytometry
<input checked="" type="checkbox"/>	<input type="checkbox"/> MRI-based neuroimaging

Unique biological materials

Policy information about [availability of materials](#)

Obtaining unique materials All unique materials are readily available from the authors.

Antibodies

Antibodies used

Mouse monoclonal ANTI- β ACTIN (Sigma-Aldrich, Cat#A5441; RRID:AB_476744, 1/5000)
 Mouse monoclonal ANTI-ATP5 β (Invitrogen, Cat#A21351; RRID:AB_221512, 1/1000)
 Mouse monoclonal ANTI-AKT (Cell Signaling Technology, Cat#2920; RRID:AB_147620, 1/1000)

Rabbit monoclonal ANTI-CCT α (Cell Signaling Technology, Cat#6931; RRID:AB_10830058, 1/1000)
 Rabbit polyclonal ANTI-EIF2 α (Abcam, Cat#ab26197; RRID:AB_2096748, 1/1000)
 Mouse monoclonal ANTI-FLAG (Sigma-Aldrich, Cat#F1804; RRID:AB_262044, 1/5000)
 Rabbit polyclonal ANTI-HIF1 α (Cayman Chemical, Cat#10006421; RRID:AB_409037, 1/1000)
 Mouse monoclonal ANTI-HSP60 (StressMarq, Cat#SMC-110; RRID:AB_2570336, 1/1000)
 Rabbit polyclonal ANTI-LC3 (Sigma-Aldrich, Cat#L7543; RRID:AB_796155, 1/1000)
 Rabbit polyclonal ANTI-LIPIN1 (Cell Signaling Technology, Cat#5195; RRID:AB_10695591, 1/1000)
 Mouse monoclonal ANTI-LIPIN1 (Santa Cruz, Sc-376874, 1/1000)
 Rabbit polyclonal ANTI-MPV17L2 (Sigma-Aldrich, Cat#HPA043111; RRID:AB_10794176, 1/1000)
 Mouse monoclonal ANTI-Myc (Cell Signaling Technology, Cat#2276; RRID:AB_331783, 1/1000)
 Goat monoclonal ANTI-OMA1 (P19) (Santa Cruz, Sc-168844; RRID:AB_10843331, 1/1000)
 Mouse monoclonal ANTI-OPA1 (BD Biosciences, Cat#612606; RRID:AB_399888, 1/1000)
 Rabbit polyclonal ANTI-PDK1 (Enzo, Cat# ADI-KAP-PK112-D; RRID:AB_2039453, 1/1000)
 Rabbit polyclonal ANTI-PISD (Abnova, Cat#PAB22508; RRID:AB_10965728, 1/1000)
 Mouse monoclonal ANTI-PRELID1 (Abnova, Cat#H00027166-M01; RRID:AB_534999, 1/1000)
 Rabbit monoclonal ANTI-pEIF2 α (S51) (Abcam, Cat#ab32157; RRID:AB_732117, 1/1000)
 Rabbit polyclonal ANTI-pS6(S235/236) (Cell Signaling Technology, Cat#2211; RRID:AB_331679, 1/1000)
 Rabbit monoclonal ANTI-RAPTOR (Cell Signaling Technology, Cat#2280; RRID:AB_561245, 1/1000)
 Rabbit monoclonal ANTI-RICTOR (Cell Signaling Technology, Cat#2114; RRID:AB_2179963, 1/1000)
 Mouse monoclonal ANTI-ROMO1 (Origene, Cat#TA505580; RRID:AB_2623202, 1/1000)
 Mouse monoclonal ANTI-SDHA (Invitrogen, Cat#459200; RRID:AB_2532231, 1/5000)
 Rabbit polyclonal ANTI-SLP2 (ProteinTech, Cat#10348-1-AP; RRID:AB_2286822, 1/1000)
 Rabbit polyclonal ANTI-STARD7 (ProteinTech, Cat#15689-1-AP; RRID:AB_2197820, 1/1000)
 Mouse monoclonal ANTI-S6 (Cell Signaling Technology, Cat#2317; RRID:AB_2238583, 1/1000)
 Rabbit polyclonal ANTI-TIMM17A (GeneTex, Cat#GTX108280; RRID:AB_2038123, 1/1000)
 Mouse monoclonal ANTI-TIMM23 (BD Biosciences, Cat#611223; RRID:AB_398755, 1/1000)
 Rabbit polyclonal ANTI-TOMM20 (Sigma-Aldrich, Cat#HPA011562; RRID:AB_1080326, 1/1000)
 Rabbit polyclonal ANTI-VDAC1 (Abcam, Cat#ab15895; RRID:AB_2214787, 1/1000)
 Rabbit polyclonal ANTI-YME1 (ProteinTech, Cat#11510-1-AP; RRID:AB_2217459, 1/1000)
 Rabbit polyclonal ANTI-4E-BP1 (Cell Signaling Technology, Cat#9452; RRID:AB_331692, 1/1000)

Validation

Validation for commercially available antibodies can be found using the links below:

Mouse monoclonal ANTI- β ACTIN; <https://www.sigmaaldrich.com/content/dam/sigma-aldrich/docs/Sigma/Datasheet/6/a5441dat.pdf>
 Mouse monoclonal ANTI-ATP5 β ; <https://www.thermofisher.com/antibody/product/ATP-Synthase-beta-Antibody-clone-3D5AB1-Monoclonal/A-21351>
 Mouse monoclonal ANTI-AKT; <https://www.cellsignal.com/products/primary-antibodies/akt-pan-40d4-mouse-mab/2920>
 Rabbit monoclonal ANTI-CCT α ; <https://www.cellsignal.com/products/primary-antibodies/ccta-d18b6-rabbit-mab/6931>
 Rabbit polyclonal ANTI-EIF2 α ; <https://www.abcam.com/eif2s1-antibody-ab26197.html>
 Mouse monoclonal ANTI-FLAG; <https://www.sigmaaldrich.com/content/dam/sigma-aldrich/docs/Sigma/Bulletin/f1804bul.pdf>
 Rabbit polyclonal ANTI-HIF1 α ; <https://www.caymanchem.com/product/10006421>
 Mouse monoclonal ANTI-HSP60; <https://www.stressmarq.com/products/antibodies/hsp60-antibody-smc-110/?v=3a52f3c22ed6>
 Rabbit polyclonal ANTI-LC3; <https://www.sigmaaldrich.com/content/dam/sigma-aldrich/docs/Sigma/Datasheet/4/l7543dat.pdf>
 Rabbit polyclonal ANTI-LIPIN1; <https://www.cellsignal.com/products/primary-antibodies/lipin-1-antibody/5195>
 Mouse monoclonal ANTI-LIPIN1; <https://www.scbt.com/scbt/product/lipin-1-antibody-b-12>
 Rabbit polyclonal ANTI-MPV17L2; <https://www.sigmaaldrich.com/catalog/product/sigma/hpa043111>
 Mouse monoclonal ANTI-Myc; <https://www.cellsignal.com/products/primary-antibodies/myc-tag-9b11-mouse-mab/2276>
 Goat monoclonal ANTI-OMA1 (P19); <https://datasheets.scbt.com/sc-168844.pdf>
 Mouse monoclonal ANTI-OPA1; <http://www.bd-biosciences.com/ds/pm/tds/612606.pdf>
 Rabbit polyclonal ANTI-PDK1; <http://www.enzolifesciences.com/ADI-KAP-PK112/pdk1-polyclonal-antibody/>
 Rabbit polyclonal ANTI-PISD; http://www.abnova.com/protocol_pdf/DS_PAB22508.pdf
 Mouse monoclonal ANTI-PRELID1; http://www.abnova.com/protocol_pdf/DS_H00027166-M01.pdf
 Rabbit monoclonal ANTI-pEIF2 α (S51); <https://www.abcam.com/eif2s1-phospho-s51-antibody-e90-ab32157.html>
 Rabbit polyclonal ANTI-pS6(S235/236); <https://www.cellsignal.com/products/primary-antibodies/phospho-s6-ribosomal-protein-ser235-236-antibody/2211>
 Rabbit monoclonal ANTI-RAPTOR; <https://www.cellsignal.com/products/primary-antibodies/raptor-24c12-rabbit-mab/2280>
 Rabbit monoclonal ANTI-RICTOR; <https://www.cellsignal.com/products/primary-antibodies/riktor-53a2-rabbit-mab/2114>
 Mouse monoclonal ANTI-ROMO1; <https://cdn.origene.com/datasheet/ta505580.pdf>
 Mouse monoclonal ANTI-SDHA; <https://www.thermofisher.com/antibody/product/SDHA-Antibody-clone-2E3GC12FB2AE2-Monoclonal/459200>
 Rabbit polyclonal ANTI-SLP2; <https://www.ptglab.com/Products/Pictures/pdf/10348-1-AP.pdf>
 Rabbit polyclonal ANTI-STARD7; <https://www.ptglab.com/Products/Pictures/pdf/15689-1-AP.pdf>
 Mouse monoclonal ANTI-S6; <https://www.cellsignal.com/products/primary-antibodies/s6-ribosomal-protein-54d2-mouse-mab/2317>
 Rabbit polyclonal ANTI-TIMM17A; <https://www.genetex.com/Product/Detail/TIMM17-antibody-C1C3/GTX108280>
 Mouse monoclonal ANTI-TIMM23; <https://www.bd-biosciences.com/ds/pm/tds/611223.pdf>
 Rabbit polyclonal ANTI-TOMM20; <https://www.sigmaaldrich.com/catalog/product/sigma/hpa011562>
 Rabbit polyclonal ANTI-VDAC1; <https://www.abcam.com/vdac1-porin-antibody-mitochondrial-loading-control-ab15895.html>
 Rabbit polyclonal ANTI-YME1; <https://www.ptglab.com/Products/Pictures/pdf/11510-1-AP.pdf>
 Rabbit polyclonal ANTI-4E-BP1; <https://www.cellsignal.com/products/primary-antibodies/4e-bp1-antibody/9452>

Eukaryotic cell lines

Policy information about [cell lines](#)

Cell line source(s)

HEK 293 cells were purchased from Invitrogen (R75007). HeLa (CCL-2), HEK293T (CRL-3216), HPAF-II (CRL-1997), PANC-1 (CRL1469) and HepG2 (HB8065) cells were purchased from ATCC. Huh7 (RRID:CVCL_0336) and MEF cells were previously sourced. References and further cell line details are included in "Supplementary Table 9".

Authentication

PDAC and HCC cell lines (HPAF-II, PANC-1, HepG2 and Huh7) were authenticated by STR profiling.

Mycoplasma contamination

All cell lines were routinely tested for mycoplasma by PCR. All cell lines were negative.

Commonly misidentified lines
(See [ICLAC](#) register)

No commonly misidentified cell lines were used.

Animals and other organisms

Policy information about [studies involving animals; ARRIVE guidelines](#) recommended for reporting animal research

Laboratory animals

BALB/cAnNRj-Foxn1 nu/nu, 6 week old, female (Janvier Labs Reference: SM-BALNU-F)

Wild animals

This study did not involve wild animals.

Field-collected samples

This study did not involve samples collected from the field.